Light in the Cave: Opal coating detection by UV-light illumination and fluorescence in a rock art context. Methodological development and application in Points Cave (Gard, France)

Marine Quiers, Claire Chanteraud, Andréa Maris-Froelich, Emilie Chalmin, Stéphane Jaillet, Camille Noûs, Sébastien Pairis, Yves Perrette, Hélène Salomon, Julien Monney

Light in the Cave: Opal coating detection by UV-light illumination and fluorescence in a rock art context

Methodological development and application in Points Cave (Gard, France)

Marine Quiers [a], Claire Chanteraud [b,c], Andréa Maris-Froelich [a], Émilie Chalmin-Aljanabi [c], Stéphane Jaillet [c], Camille Noûs [e], Sébastien Pairis [d], Yves Perrette [c,b], Hélène Salomon [c], Julien Monney [c]*

[a]*Laboratoire Commun SpecSolE, Envisol – CNRS - Univ. Savoie Mont Blanc, Chambéry, 73000, France*
[b]*Missouri University Research reactor - University of Missouri 65203 Columbia MO*
[c]*EDYTEM UMR5204, CNRS, Univ. Savoie Mont Blanc, Chambéry, 73000, France*
[d]*Univ. Grenoble Alpes, CNRS, Grenoble INP, Institut Néel, Grenoble, 38000, France*
[e]*Laboratoire Cogitamus, 1 ¾ rue Descartes, Paris, 75005, France*

** Corresponding author: m.quiers@envisol.fr*

Abstract

Silica coatings development on rock art walls in Points Cave questions the analytical access to pictorial matter specificities (geochemistry and petrography) and the rock art conservation state in the context of pigment studies. However, classical *in situ* spectroscopic techniques appear unsuccessful to identify these coatings, which also prevent pigment characterization. In this study, we propose using a UV fluorescence method for opal coating detection based on the fluorescence specificities of uranyl-silica complexes composing these deposits. A coupling of spectral identification using UV laser-induced fluorescence spectroscopy with UV illumination was performed on samples and µ-samples from the Points Cave rock art site. The well-defined peaks observed in fluorescence emission spectra due to uranyl ions validate opal detection and its correspondence with green fluorescence observed under UV light at micro- and macroscopic scales. *In situ* optical measurements under UV illumination reveal the presence of opal coating, especially on rock art walls in Points Cave. Opal occurrence and repartition observations provide the first insights into Points Cave wall evolution and chronological constraints linked to opal coating development. Regarding the strong interactions with pigment

suggested by multiscale observations of samples and µ-samples, the impact of the presence of opal coating on Points Cave rock art conservation quality is questioned. Thus, by developing a specific and non-destructive characterization method for opal coatings, this study opens up a new approach for the study of decorated wall taphonomy and proposes utilizing mineralization both as markers of the natural history of caves and as an indication for their uses by ancient human groups.

Keywords: Silica coating, uranyl, UV fluorescence, *in situ* detection, rock art, Quaternary, archaeology, Ardèche, France, optical methods

1. Introduction

Natural activity in caves, mostly water weathering (Delvigne, 1998; Chalmin *et al.*, 2019; Salomon *et al.*, 2021), transforms the surface of the walls by physical, chemical, biological and mechanical action. Thus, the traces of all these transformations (environmental input) can be a source of information regarding natural and anthropological events on the wall surface, such as drawing and painting realizations, cave environment evolution, and human presence in the cave (Sadier, 2013; Pons-Branchu *et al.*, 2014; Quilès *et al.*, 2015; Shao *et al.*, 2017; Valladas *et al.*, 2017; Monney & Jaillet, 2019).

Among the taphonomic processes impacting rock art pictorial matter, mineral-coating formation as weathering products is well described in rock art research (Vignaud *et al.*, 2006; Huntley, 2012; Bassel, 2017; Chalmin *et al.*, 2018; Mauran *et al.*, 2019). Silica rich amorphous deposits, also called silica skins, have been observed at different cave and open-air rock art sites (Watchman, 1990; Aubert *et al.*, 2004; Aubert *et al.*, 2012; Huntley, 2012). Those studies have suggested both a positive and negative impact on rock art conservation due to opal coating development. Indeed, the strong interaction suspected with hematite pigments has been suggested as an element of conservation

enhancement, notably compared with other pigments (Watchman, 1990). However, some authors have also observed exfoliation processes of silica skins, which could play a role in rock art weathering (Aubert *et al.*, 2004; Green *et al.*, 2017). To our knowledge, there is still no clear answer on the role of silica coatings as conservation factors of pictorial matter. In addition to this conservation issue, silica skins have been proposed as tools for indirect dating of rock art, especially in the case of inorganic pictorial matter (Aubert *et al.*, 2004; Aubert *et al.*, 2012). Indeed, this mineral phase is known to be enriched in uranyl ions, but the U-Th dating application remains hypothetical due to silica skin thickness and absence of stratigraphy, which complicate both sampling and measurement reliability (Green *et al.*, 2017).

Thus, silica skin characterization represents a key issue in the context of rock art studies. However, it remains difficult to identify and characterize, especially with non-invasive techniques. Currently, the use of *in situ* spectroscopic techniques in rock art studies is increasing, as these methods can provide information on both pictorial matter and pigment environments (substrate, deposits, concretions, etc.). The portability and decreasing cost of instruments coupled with the rapidity and the non-destructive character of analyses have led to a quasi-systematic use of these techniques in recent rock art studies (Huntley, 2012, Mauran *et al.*, 2019; Trosseau *et al.*, 2021; Chanteraud *et al.*, 2021). However, amorphous silica characterization, even in rock art context, is generally based on laboratory observations such as SEM or XRD analyses (Watchman, 1990; Gaillou *et al.*, 2008; Garcia-Guinea *et al.*, 2013; Huntley *et al.*, 2015; Green *et al.*, 2017). In addition, the signal of pictorial matter acquired with portable spectroscopic techniques could be impacted by the presence of silica skins, as observed by Huntley (2012) in the case of pXRF measurements.

In this paper, we propose a new method for *in situ* detection and characterization of amorphous silica in a rock art context based on UV laser-induced fluorescence (LIF). Indeed, uranyl fluorescence characteristics under UV light are well known and have been observed in silica mineralization, especially in opal (deNeufville *et al.*, 1981; Gorobets *et al.*, 1977; Fritsch *et al.*, 2001; Gaillou *et al.*,

2008). UV spectroscopy presents the same advantages as other portable spectroscopic techniques, but the bright green fluorescence and the specific spectral features displayed by uranyl ions enable the targeted identification of opal coatings. To our knowledge, only one study has reported opal detection in caves using optical methods based on UV techniques (Garcia-Guinea *et al.*, 2013), and no study has applied UV spectroscopic methods in a rock art context for opal identification. Here, we propose a methodological development based on laboratory and field experiments to validate the use of *in situ* UV techniques for opal detection in a rock art context by coupling *in situ* optical and spectroscopic analyses to obtain multiscale information.

This study was performed in Points Cave (Aiguèze, Gard, France), which contains an important spread of opal coating on the cave walls. In this approach, Points Cave perfectly illustrates the importance of environmental input characterization in the study of rock art (Chanteraud et al., 2021). In Points Cave, some pieces of the rock wall bearing colouring matter were discovered during archaeological excavations in front of some rock art panels which allowed transport, µ-sampling and analysis in the laboratory. Analysis of these coloured flakes allows us to identify and measure the environmental input, which modifies and obscures the identification of pictorial matter characteristics.

2. Material

2.1 Study site: Points Cave

Located in the Ardèche River Canyon, less than 10 km downstream of Chauvet Cave, Points Cave is a Palaeolithic rock art site identified in 1993 (Figure 1) (Deschamps *et al.*, 2018). Archaeological studies have been performed since 2011 as part of the "Datation Grottes Ornées" project ("Cave Art Dating" project, Monney, 2011; 2018). The entrance opens on a hundred-metre long cave in Urgonian limestone. The rock art which is exclusively composed of red drawings and paintings, is located in the middle part of the cave preserved from sunlight (Figure 1). Excavations conducted at the entrance

indicated human and animal occupation since the late Pleistocene to the present day (Monney & Jaillet, 2019).

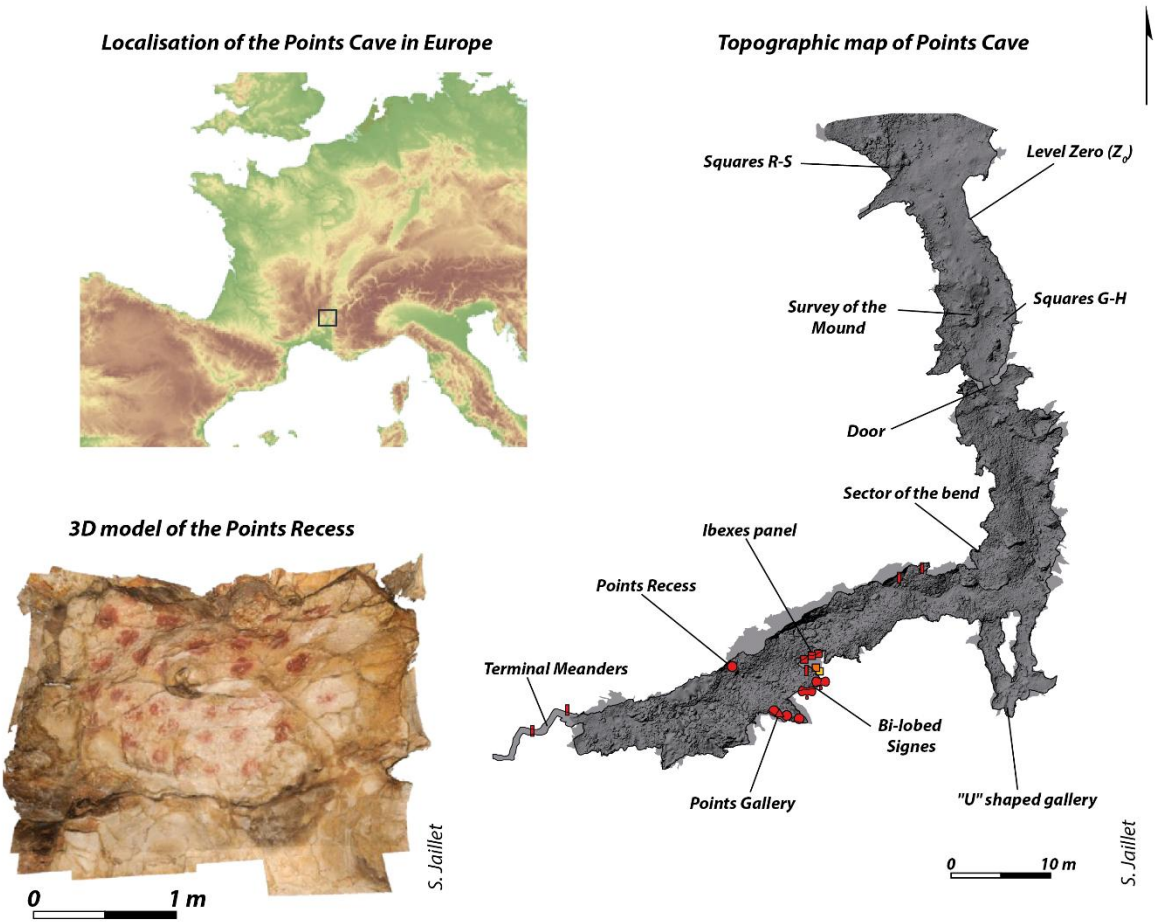

Figure 1*: Points Cave location in southeastern France, topographic map of the cave with location of the excavations and the rock art panels (J. Monney); 3D model of the "Points Recess" panel (J. Monney)*

Points Cave is currently disconnected from hydrogeological flows (Jaillet & Monney, 2018). Only a few infiltrations can be observed after strong precipitation events. The low level of leaching on the wall and the low relative presence of a calcite veil are due to this weak hydrogeological activity. Millimetric to centimetric concretions and efflorescence's (coralloid type of crystallization) have also

developed on the wall surface in the rock art sector (Mauran, 2019 in Monney et al., 2019; Barbaran & Nouet, 2020).

2.2 Points Cave rock art and pictorial matter

Rock art, composed exclusively of red drawings and paintings, is currently observed in the middle part of the cave. It comprises five animal figures (3 ibexes, 1 horse, 1 bison), five indeterminate tracings, two bi-lobed signs, one open-angle sign and four clusters containing a total of 59 palm-printed dots, commonly referred to as "palm dots" (Monney, 2018). On-site spectroradiometric analysis showed that Points Cave rock art is homogenous in colour (Lafon *& al.*, 2022). Moreover, pieces of colouring matter were found during the archaeological excavations in the sedimentary sequence at the entrance of the cave (Chanteraud *et al*., 2019; Chanteraud, 2020).

Investigations carried out at the foot of the rock art panel known as the "Bi-lobed Signs" revealed the presence of five coloured wall flakes on the ground in the chaos of rocks: S-ECA-01 to S-ECA-05. These 3 to 20 cm flakes are composed of limestone fragments detached from the wall by mechanical action and covered on one side with colouring matter (Monney, 2011). They more than likely come from the large bilobed sign (PTS-10) or from other unknown rock art that may have crumbled entirely from the walls nearby (Monney, 2018). These flakes are a major asset of Points Cave because they allow to investigate the cave walls surface with accurate instruments by bringing them in the laboratory.

To identify both the iron-oxide morphologies and the natural mineralization that can form on the surface of the decorated walls, our study was focused on three of the five wall flakes (S-ECA-03, S-ECA-04, S-ECA-05) discovered in the rock art sector of Points Cave, because of the presence of opal

coating on their surface (Figure 2). µ-sampling of pictorial matter was performed on the coloured flakes: µ-S-ECA-03, µ-S-ECA-04, µ-S-ECA-05. These last two have been fragmented during sampling giving: µ-S-ECA-04_prlvt_01, µ-S-ECA-04_prlvt_02 and µ-S-ECA-04_prlvt_03, and µ-S-ECA-05_prlvt_01 and µ-S-ECA-05_prlvt_02 (S.I.1).

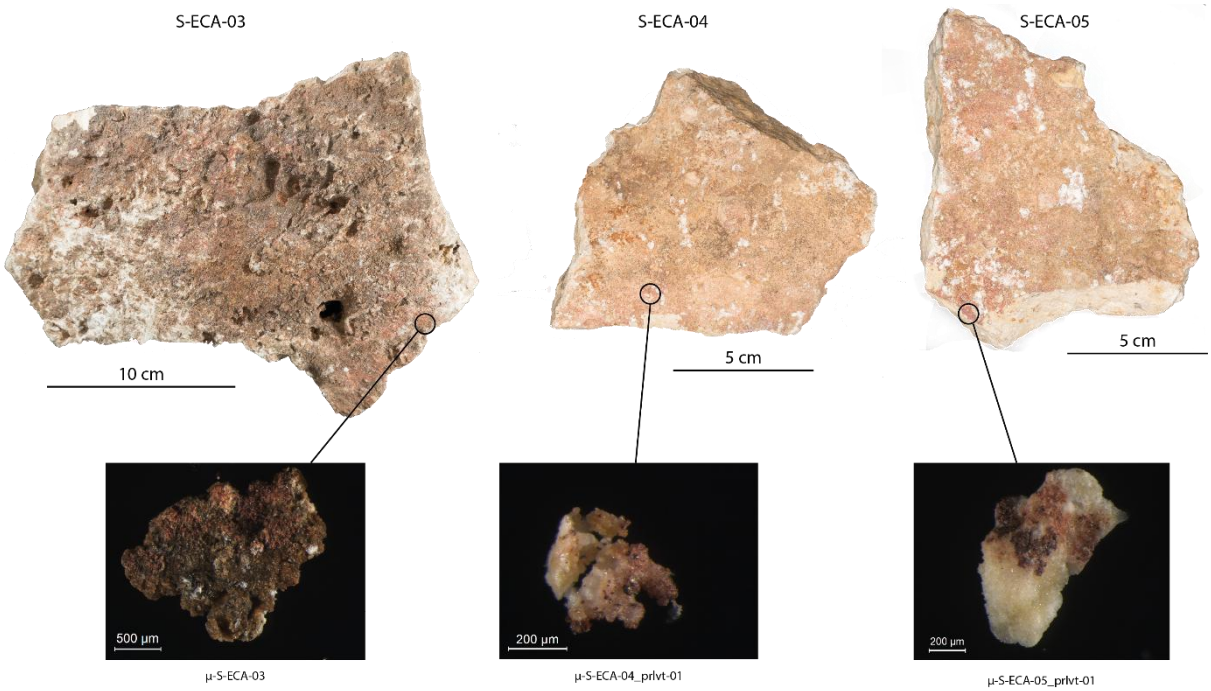

***Figure 2**: Limestone flakes found in the archaeological excavations at the foot of the Bi-lobed Signs panel and location of µ-sampling.*

Moreover, 12 µ-samples of pictorial matter on limestone and 8 µ-samples of the undecorated cave walls (limestone) were directly sampled on and/or around the rock art panels of the cave and added to the study (Table 1, S.I.2). All µ-samples of pictorial matter were observed and analysed without any preparation.

***Table 1**: Inventory of µ-samples with colouring matter coming from the rock art panels*

Sample N°	***Rock Art***	***Type***
	– Ibexes Panel –	
Prm-19-01	*Near to the Ibexe n°5*	*Wall Blank*
Prm-19-02	Ibex n°5	Pictorial matter
	– Horse Panel –	
Prm-19-03	*Near to the Horse*	*Wall Blank*
Prm-19-04	Horse n°7	Pictorial matter
Prm-19-05	Bison n°8	Pictorial matter
	– Bi-lobed Signs Panel –	
Prm-19-06	*Near to the Sign n°9*	*Wall Blank*
Prm-19-07	Small Bi-lobed Sign n°9	Pictorial matter
Prm-19-08	Large Bi-lobed Sign n°10	Pictorial matter
Prm-19-09	Palm-dot n°14-02	Pictorial matter
Prm-19-10	Open-angle Sign n°13	Pictorial matter
	– Dots Galerie –	
Prm-19-11	*Near to the Palm-dot n°11-02*	*Wall Blank*
Prm-19-12	Palm-dot n°11-02	Pictorial matter
Prm-19-13	Palm-dot n°11-03	Pictorial matter
	– Dots Gallery (cluster 11) –	
Prm-19-14	*Near to the Palm-dot n°11-01*	*Wall Blank*
Prm-19-15	Palm-dot n°11-01	Pictorial matter
Prm-19-16	Palm-dot n°15-21	Pictorial matter
Prm-19-17	Palm-dot n°15-01	Pictorial matter
	– Points Recess –	
Prm-19-18	*In the center of the panel*	*Wall Blank*
	– Between Ibexes panel and Horse panel –	
Prm-19-19	*On the limestone*	*Wall Blank*
	– Points Recess –	

175

176

177 **3. Methods**

178

179 **3.1 Macroscopic and microscopic observations**

180

181 *3.1.1 Laboratory and in situ observations at macroscopic scale*

182

183 Image capture for macroscopic observations was performed in two steps: 1) a photograph was taken
184 under white light, and 2) another photograph was taken under UV light illumination. Observations at
185 macroscopic scale in the laboratory and in the cave were realized with a Canon EOS 5D Mark III
186 camera and a Canon EOS 7D camera fixed on a tripod. A detached flash was used for image capture
187 under white light. For UV light illumination, 4 UV LEDs (280 nm, 2.26 W, NewEnergy) were fixed
188 on orientable macroflash bars on each side (2 LEDs per side) of the camera, allowing both
189 macrophotography and general views of cave walls. Camera parameters are available in Table 2.

190

Table 2*: Camera parameters used for both white and UV light illumination during field and laboratory macroscopic observations.*

			Aperture	*Obturation speed (sec)*	*Iso*
Laboratory	White light		F/7.1	1/320	1600
	UV light		F/7.1	10	1600
Field	White light	*Macro*	F/11	½	320
		Wall view	F/11	1/60	100
	UV light	*Macro*	F/4.5	½	320

Wall view	F/11	15	320	

Laboratory observations were also performed using a stereomicroscope (LEICA M165 C) under white and UV light. The same 4 LEDs were used for UV illumination.

3.1.2 Laboratory observations at microscopic scale

At microscopic scale, observations of µ-samples of flakes on carbon tape were realized with a field-emission scanning electronic microscope (SEM) ZEISS Ultra+ associated with an EDX (energy dispersive X-ray) probe (SDD, Bruker) working in high-vacuum mode with a 15 keV voltage. Images were taken with secondary electrons using in-lens or Everhart-Thornley detectors (SE2) and with backscatter electrons (BSE-AsB detector) (Néel Institut, Grenoble).

3.2 UV fluorescence analyses

Stationary fluorescence signal of flake and flake µ-samples was measured in the laboratory with a solid-phase spectrofluorimeter designed in the EDYTEM laboratory for non-destructive solid-phase measurements (Perrette *et al.*, 2000).

This instrument is divided into excitation and detection compartments associated with a translation stage system for sample surface measurement. For this experiment, the excitation system was composed of a Nd:YAG laser (Crylas, FQSS266-Q1) with a 266 nm excitation wavelength. The fluorescence emission response was collected after sample excitation by focusing the laser beam (~30 µm) on its surface. The detection system was composed of a low-pass filter monochromator (Jobin Yvon, MicroHr) for light diffraction, fitted with a 300-g/mm diffraction-grating centred at 620 nm, associated with a thermoelectric-cooled, back-illuminated CCD (Jobin Yvon, Sincerity) for high-efficiency signal detection in the UV-visible light domain. As no manipulation, modification or

destruction of the sample surface occurred during analysis, this technique is suitable for archaeological sample measurements.

Two types of fluorescence measurements were realized:

- Single point measurements were performed on flake µ-samples: µ-S-ECA-03, µ-S-ECA-04 and µ-S-ECA-05-02 (S.I.3). One spectrum was independently acquired on the sample. Measurement location was determined manually. An acquisition time of 1 s and a monochromator entrance slit of 0.25 mm (~1 nm spectral resolution) were used for spot spectrum acquisition.
- Surface measurement was performed on flake S-ECA-05 (S.I.4). The motorized translation stage system allowed movements in two directions for surface measurements. The image was obtained by stacking lines along the Y-axis. For this study, fluorescence surface imaging was performed with a 100×100 µm resolution using a 0.1 s acquisition time and a 0.05 mm entrance slit.

Data pre-processing was performed with MATLAB software (S.I.5). Spectra were corrected from baseline and instrument responses and then filtered with the Savitsky-Golay method (Savitzky & Golay, 1964).

4. Results

4.1 Macroscopic scale observations

At macroscopic scale (by visual inspection), beside the centimetric coralloid crystallization there is no other mineralization visible than the limestone on the walls, flakes or µ-sample surfaces. In fact, at this observation scale, surfaces seemed to be well preserved with strong colouration from the pictorial matter and clear access to the calcareous substrate (Figure 2).

Despite the results of the visual inspection of the walls and the observation of the µ-samples both of the rock art and the flakes under stereomicroscope, pXRF analyses (1 cm^3 spot) showed that decorated panels of the cave display mineralization, such as calcium sulphate (Chanteraud *et al.*, 2020; S.I.6). This contradiction between observation and geochemical analysis reveals the need for microscopic inspection using SEM device.

4.2 Microscopic scale observations

At the microscopic scale, a 1 µm-thin mineral film consisting of nonordered spheres was identified as silica mineralization on µ-S-ECA-03, µ-S-ECA-04-prlvt-02, µ-S-ECA-05-prlvt-01 (Figure 3; S.I.2). However, µ-S-ECA-03 shows less opal coating than the two other µ-samples. The geochemistry and hummocky morphology of the opal could be related to a type A-g amorphous opal with a SiO_2nH_2O formula (Flörke *et al.*, 1991). The mineral structure present on coloured flakes suggests its formation from a water film containing a high concentration of silica (Monger & Kelly, 2002; Curtis *et al.*, 2019). With this mode of formation, it is difficult to assume if the opal came before the hematite deposit. In fact, it is possible that the opal coating grows at the interface between the limestone substrate and the colouring matter.

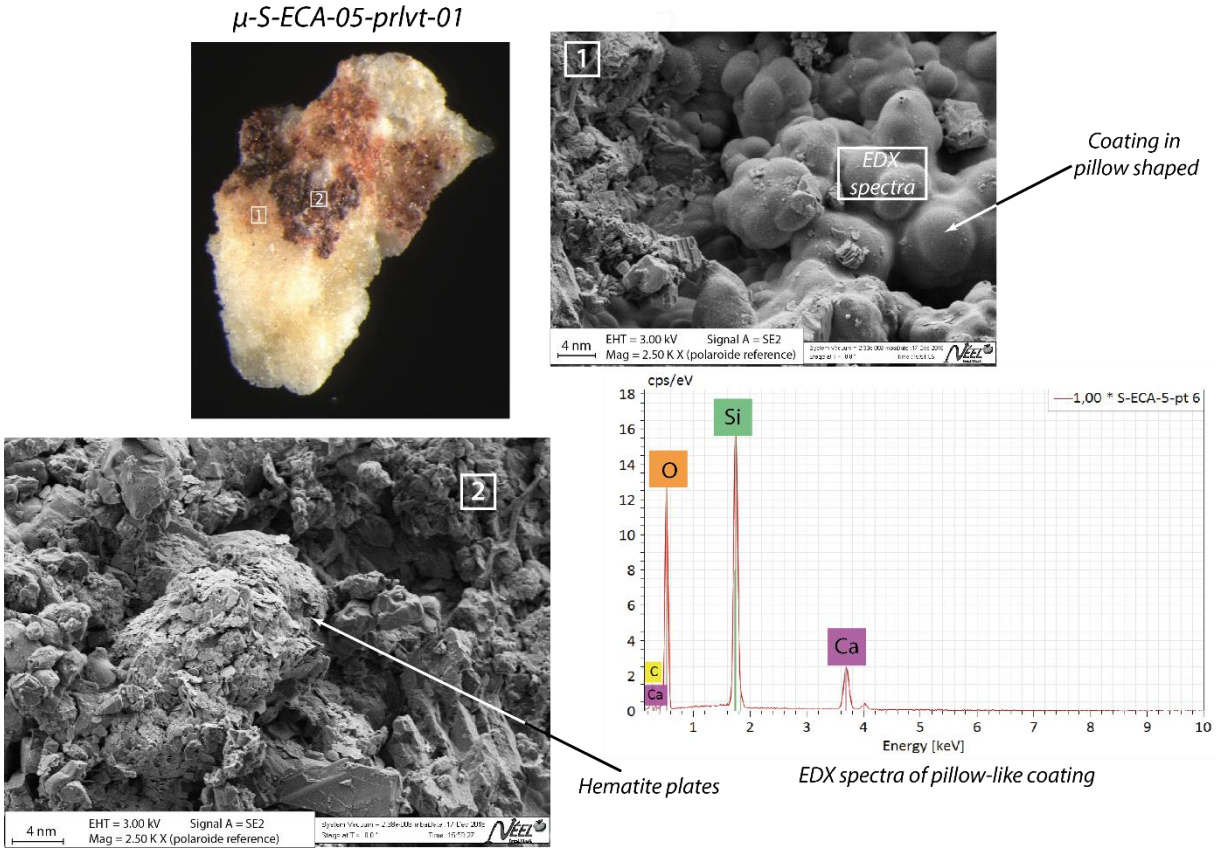

***Figure 3**: SEM observations of μ-S-ECA-05_prlvt_02. 1/ Hematite plate observation in Secondary Electron mode (SE); 2/ Pillow-like silica coating on surface in SE mode; White rectangle = Area of EDX spectra on the pillow-like silica coating.*

Concerning the μ-samples directly collected on the decorated walls, the same observations were noted, including pseudohexagonal platy hematite and strong indications of opal (S.I.1). Importantly, these samples showed significant opal development, with a complete coating of the pictorial matter to the extent that the morphology of the hematite was no longer observable on the surface (Figure 3). Weathered hematite plates seem to have been "ingested" by the silicate coating and could only be observed when a section was accessible on the surface of the sample (Figure 4 + S.I.2). However, preliminary studies on the walls of Points Cave using portable spectroscopic techniques (pXRF and Raman) could not identify the presence of opal coating *in situ* (Chanteraud *et al.*, 2020).

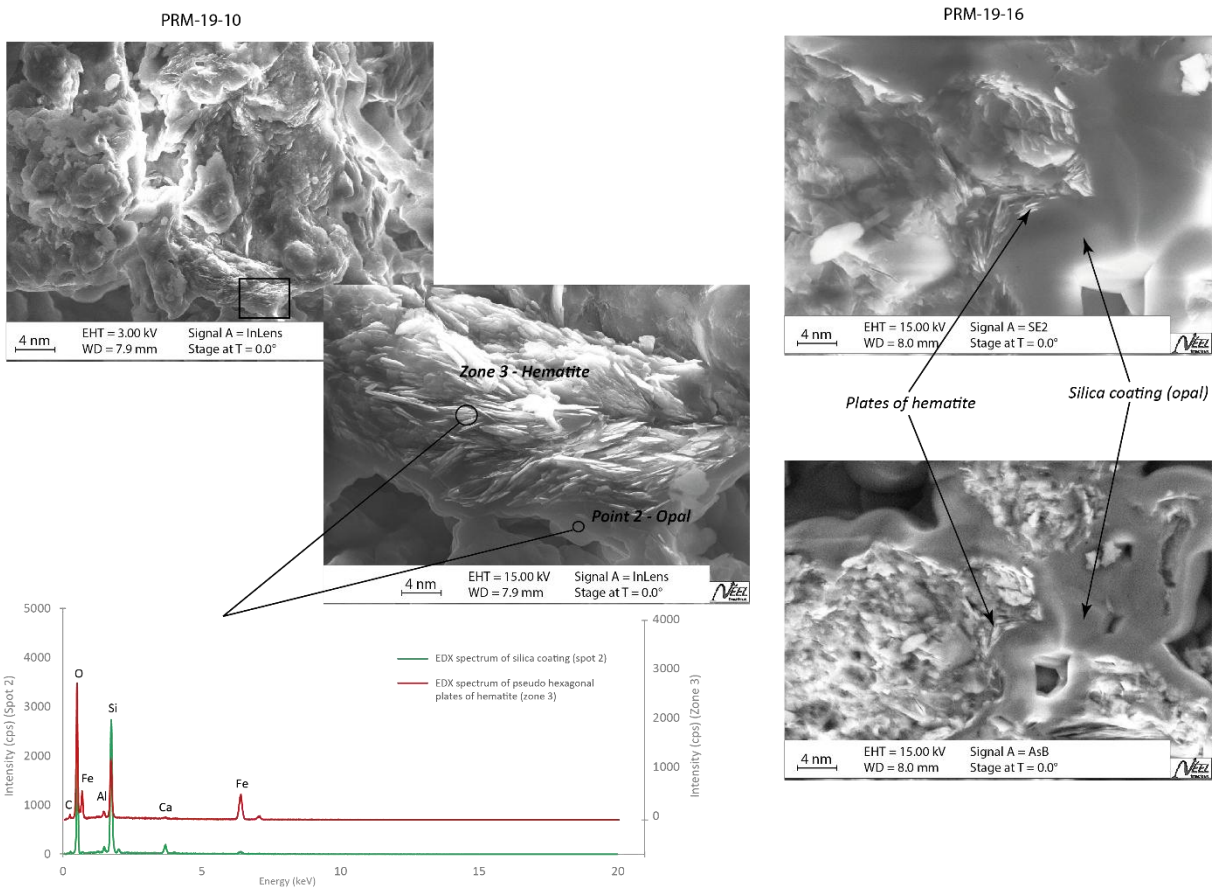

Figure 4*: Hematite plates embedded in the silica coating on PRM-19-10 and PRM-19-16 µ-samples (SEM observation in SE and BSE mode).*

4.3 Opal identification by UV-fluorescence

Fluorescence analyses were first performed on 3 flake µ-samples (µS-ECA-03, µS-ECA-04 and µS-ECA-05) that were previously characterized by different geochemical analyses and on which opal was detected. Due to the small size of the samples (approximately 200 µm), only a few localized spectra were recorded. The spectra obtained could be divided into different emission regions depending on the main signal sources (Figure 5, S.I.3):

- From 300 to 470 nm, this region corresponds to the fluorescence emission of the sample matrix.

Peaks and shoulders were detected at approximately 350 nm, 380-390 nm, 410 nm and 430-440 nm. According to the literature, they could be associated with organic matter entrapped in the crystalline matrix (McGarry & Baker, 2000; Perrette *et al.*, 2000; Van Beynen *et al.*, 2001; Perrette *et al.*, 2005; Quiers *et al.*, 2015) or with the silica material fluorescence response to UV-light excitation (Boyko *et al.*, 2011; Garcia-Guinea *et al.*, 2013).

- From 470 to 750 nm, special features were identified in this part of the spectra for samples µS-ECA-04 and µ-S-ECA-05. They were characterized by a sequence of 3 defined peaks at 501, 521, and 545 nm and a shoulder at approximately 572 nm. These peaks were identical in all spectra measured on µ-samples µS-ECA-04 and µ-S-ECA-05 and coincided with the uranyl ion spectrum in silica matrices based on a review in the literature (Table 3), but were absent from µ-S-ECA-03 spectra.

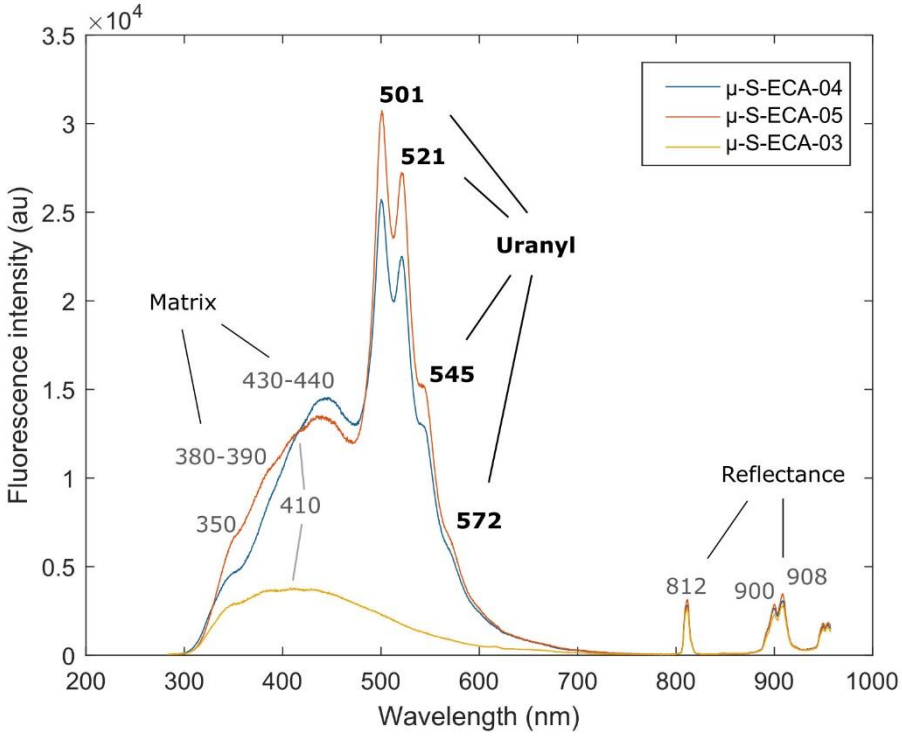

Figure 5*: Mean fluorescence emission spectra (excitation: 266 nm) of samples µ-S-ECA-04, µ-S-ECA-05 and µ-S-ECA-03. Spectra are divided into three different regions as a function of the main*

fluorescence signal sources: sample matrix, uranyl ions and laser emission reflectance.

Entrapment of uranyl ions in siliceous matrices, especially opal phases, is well documented in the literature (Zielinski, 1980; Kasdan *et al.*, 1981; Kinnunen & Ikonen, 1991; Neymark *et al.*, 2000; Fritsch *et al.*, 2001; Gaillou *et al.*, 2008; Devès *et al.*, 2012; Fritsch *et al.*, 2015; Othmane *et al.*, 2016). The strong affinity of uranyl groups for amorphous silica leads to a strong U-opal association, which is stable at the scale of geological time (Othmane *et al.*, 2016). As opal was the only silica phase identified on these samples, uranyl-specific spectra could be associated, in this case, with the presence of opal on samples, and UV fluorescence analysis represents an efficient tool for its identification.

As opal detection was subject to uranyl fluorescence properties, detection using UV fluorescence was dependent on uranium entrapment in silica crystalline structures. In their study of opal gems from different geographic and geological contexts, Gaillou *et al.* (2008) showed that not all opals are fluorescent. Opal fluorescence can be divided into two classes: blue fluorescence caused by intrinsic oxygen-related defects typical of amorphous silica structures and green fluorescence attributed to uranyl groups (Fritsch *et al.*, 2001, 2003), which is believed to be typical of common opals. A low content of U ($\geq$ 1 ppm) automatically induces a green fluorescence response to UV light excitation. This content can reach more than 100 ppm in some deposits (Gaillou *et al.*, 2008). Garcia-Guinea *et al.* (2013) measured a uranium amount of 193 ppm in stalactites in Castañar Cave. Thus, detection of opal via UV fluorescence is not systematic but common, as a low content of uranium allows fluorescence emission. However, uranium concentration in Points Cave µ-samples have not been measured due to the particularly thin opal layer and the impossibility of destroying µ-samples.

Table 3*: Fluorescence emission peaks for different opal or amorphous silica deposits reviewed in the literature.*

	Fluorescence emission peaks (nm)

Othmane *et al.* 2016	504	524	546	570	-
	504	523	545	573	-
Fritsch *et al.* 2015	504	524	546	572	604
Brennan & White 2013	502	520	-	-	-
Garcia-Guinea *et al.* 2013	505	524	543	569	-
This study	**501**	**521**	**545**	**572**	-

325

326 *4.4 Opal visual detection under UV light*

327

328 As explained previously, minerals containing uranyl ions (UO_2^{2+}) have been known to exhibit strong
329 fluorescence marked by specific spectral features and temporal characteristics since at least early 1900
330 (deNeufville *et al.*, 1981). The bright green fluorescence of uraniferous opal is a well-known
331 characteristic of this mineral phase and has been related to the presence of uranium (Gorobets *et al.*,
332 1977; Fritsch *et al.*, 2001). To evaluate whether this specificity can be used for opal detection, flake µ-
333 samples were exposed to UV light (see 3.1.1). The results show that µ-samples µ-S-ECA-04 and µ-S-
334 ECA-05 exhibited a bright green-light response (Figure 6). These two sample spectra contained
335 specific features corresponding to the fluorescence emission of uranyl ions. Green illumination was
336 thus associated with the presence of U-opal on these samples. The case of µ-sample µ-S-ECA-03 was
337 more complex. In this case, the absence of uranyl characteristic peaks in fluorescence spectra can be
338 attributed to the low opal occurrence on the µ-sample surface as observed with SEM. However,
339 localized greenish fluorescence could be distinguished on the sample under UV light illumination.
340 This could be explained by a less precise measurement due to a more difficult targeting of opal
341 because of the higher sample size or more scattered opal distribution. Second, the sample surface was
342 more coloured and had more pictorial matter (cf. §4.1), suggesting decreased ability for detection.

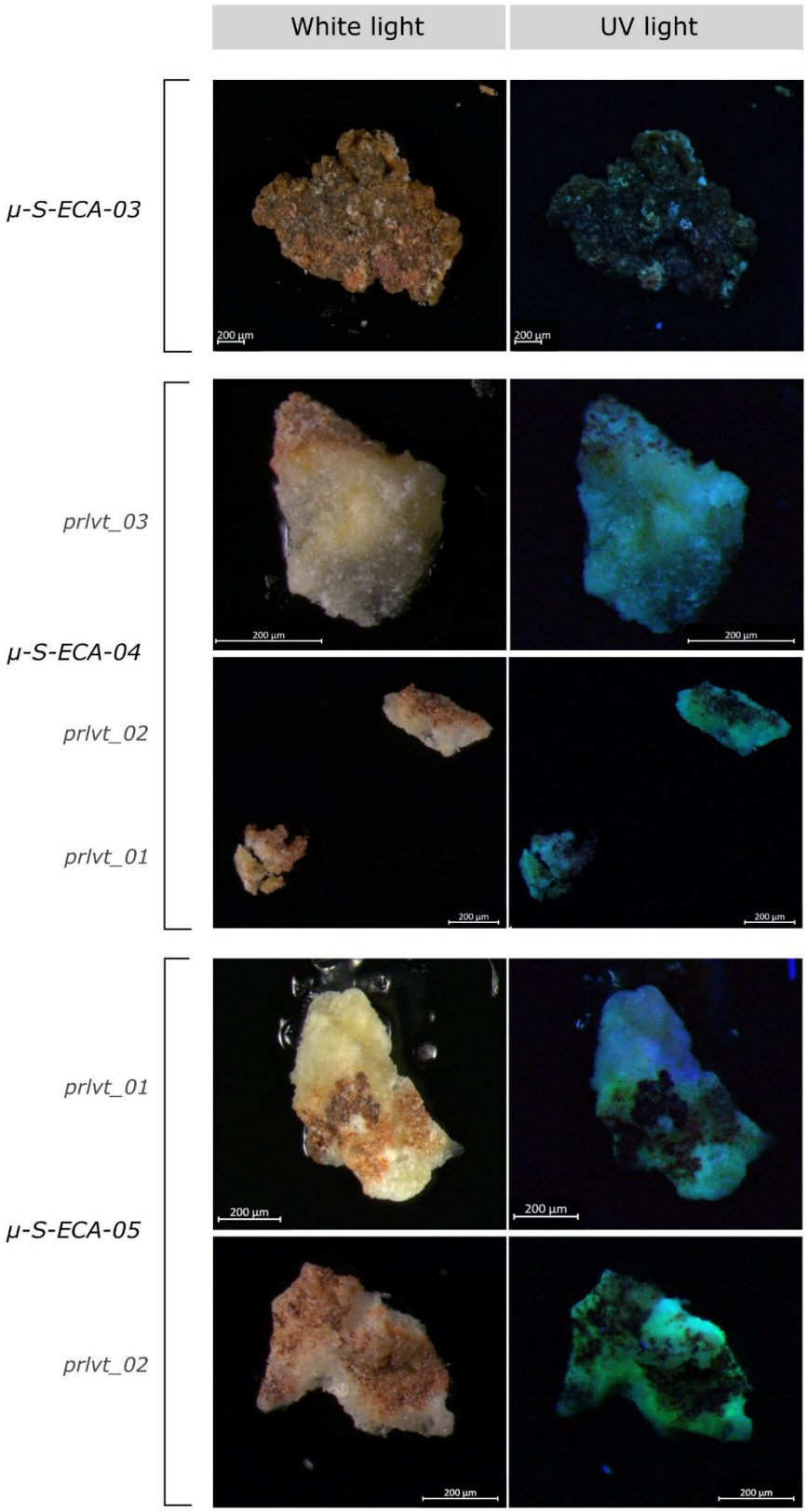

343

***Figure 6**: Photographs of µ-samples taken on flakes under white and UV light.*

4.4 From the lab to the cave

4.4.1 Comparison between UV methods

Considering that uranyl green illumination is representative of the presence of opal, detection concordance between spectral and visual techniques was tested at a larger scale by comparing UV-illuminated photographs with UV fluorescence cartography of flake S-ECA-05.

First, to evaluate UV LIF method accuracy at a larger scale, a second experiment was performed directly on flake S-ECA-05. UV fluorescence cartography (100 x 100 µm resolution, S.I.4) showed a range of spectra presenting uranyl spectral characteristics. Indeed, uranyl peaks present different intensities or ratios compared to the fluorescence signal of the matrix, or cannot be detected. Assuming that the fluorescence signal can be interpreted as a mixing of a uranyl signal with a global matrix signal, opal information was extracted from fluorescence cartography using a mixing algorithm, MCR-ALS, with the MCR-ALS toolbox in MATLAB software (Jaumot *et al.*, 2015). MCR-ALS has become a popular chemometric method in solving mixture analytical models. It is based on an additive bilinear model of pure contributions that depends on the concentration and the specific spectral sensitivity of each component. This algorithm can also be applied to obtain quantitative information (Jaumot *et al.*, 2005; de Juan *et al.*, 2014; Zhang & Tauler, 2013).

A singular value decomposition (SVD) method was first applied on the entire raw dataset in the MCR calculation to define the number of initial loadings (S.I.5). Based on the eigen values obtained with the SVD method, three components were graphically determined as mainly contributors to the fluorescence signal and represent 76.8% of the explained variance. These three initial loadings were then calculated in the MCR-ALS method using the PURE algorithm, a commonly used method to find the purest variable. MCR-ALS was then performed based on these 3 initial loadings on the same entire

dataset. Non-negativity constraint was applied for model optimization. For each spectrum, model results (r^2=99.8) provided a proportion of each recalculated loading (Figure 7). The second loading represents the uranyl spectrum from which is calculated a proportion of uranyl contribution to the total fluorescence signal. This contribution can be associated with a proportion of opal at the sample surface for each pixel as presented in Figure 7. The other loadings correspond to the contribution of different fluorescence parts in the spectra related to the matrix fluorescence (loading 3) and to some specific highly intense signals at the sample surface (loading 1), probably due to particular minerals.

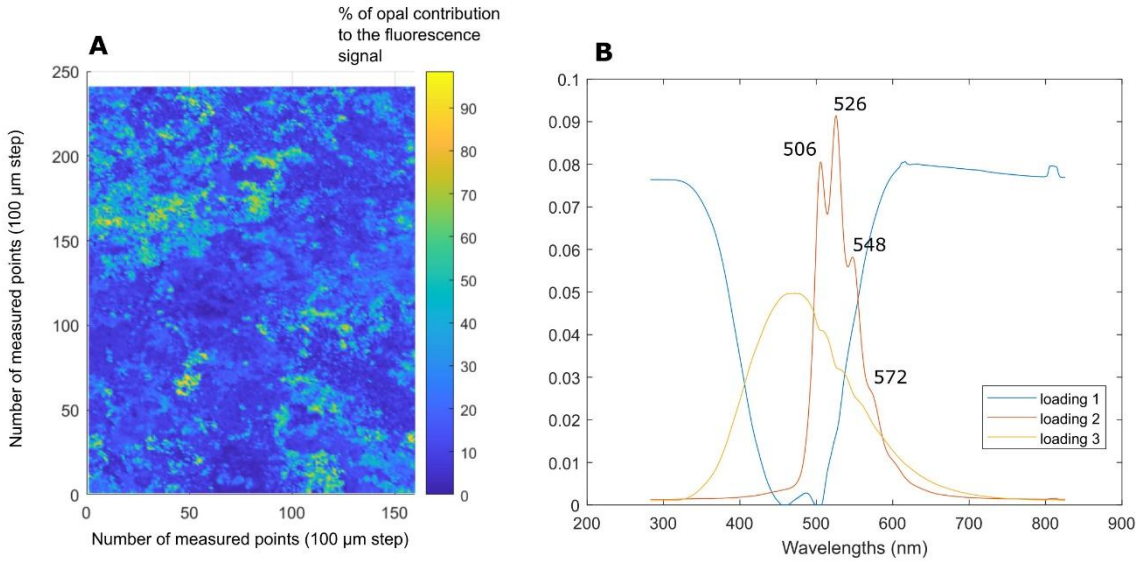

Figure 7*: MCR-ALS results: A/ Representation of the proportion of opal in the total fluorescence signal calculated from loading 2 on the S-ECA-05 surface, B/ Loadings obtained after model optimization.*

Evaluation of opal proportions on the sample using this method is, however, subject to certain biases. Similar to the majority of spectroscopic techniques, this detection method can only detect surface deposits. Thus, opal mineralization located under other mineral or organic deposits cannot be detected. Moreover, for quantitative measurement, the measurement sensitivity to changes in sample surface

385 microtopography must be taken into account. As the laser beam is focused on the surface, variations in
386 fluorescence intensities measured on the sample, and thus opal estimations, can be biased by
387 millimetric changes in surface relief.
388
389 This method remains effective in extracting information on opal mineralization even on heterogeneous
390 matrices, such as the Points Cave µ-samples. Due to its specific spectral shape, uranyl signal can be
391 easily extracted from mixed fluorescence signals. Mixing algorithms could provide quantitative
392 information if combined with calibration methods. Indeed, the MCR-ALS algorithm has been used for
393 the quantification of different target molecules based on various spectroscopic data (Mas *et al.*, 2010;
394 Araya *et al.*, 2017; Kumar *et al.*, 2018; Castro *et al.*, 2021). Regarding sample complexity, calibration
395 protocols based on standard references and prepared or artificial mixtures are difficult to apply (Araya
396 *et al.*, 2017). Quantification strategies need to be developed for archaeological materials, reaching a
397 balance between sample destruction and model result robustness, such as those developed for
398 hyperspectral data. Then, the estimated concentration accuracy will depend on the legitimacy of the
399 assumption made in the quantification strategy (Araya *et al.*, 2017).
400
401 For field purpose, opal information provided by UV illumination and UV LIF methods were
402 compared. The green component of the RGB image was extracted from UV-light photos. The
403 grayscale image was subtracted to avoid the luminosity effect, and a threshold was applied to the
404 image obtained to select only pixels containing green colour (S.I.5). To help compare the opal
405 information provided by both techniques, images were aligned using point control selection and
406 geometric transformation functions in MATLAB.
407
408 The results show a high correspondence between spectral and visual detection methods (Figure 8). To
409 evaluate the efficiency of the optical method, opal cartographies with different detection limits were
410 simulated by modifying lower boundaries to select pixel associated with opal presence. These
411 boundaries are based on % of opal contribution to the fluorescence signal for spectroscopic

412 measurements. The best correlation coefficient (R^2=0.50) is obtained for an opal contribution
413 threshold of 25% of the total fluorescence signal. Graph D on figure 8 shows that optical method was
414 the most efficient when opal fluorescence emission contributed at least from 20% to 43% of the total
415 fluorescence signal of the sample. If the opal proportion limit for pixel selection is settled too low, the
416 number of pixels selected is too important to provide a good correlation and conversely. For example,
417 80% of pixels in the image were selected with a limit settled from 8% of opal contribution, providing a
418 correlation coefficient of only 0.24. The rather low correlation coefficient between both images could
419 mainly be explained by the point control selection and geometric transformation applied to readjust
420 them together. Angle disposition of the sample and detector combined with image resolution could
421 have led to difficulties in adjusting the images. Further research in the computational image domain
422 could improve the methodology and enhance the correlation between the two techniques.
423

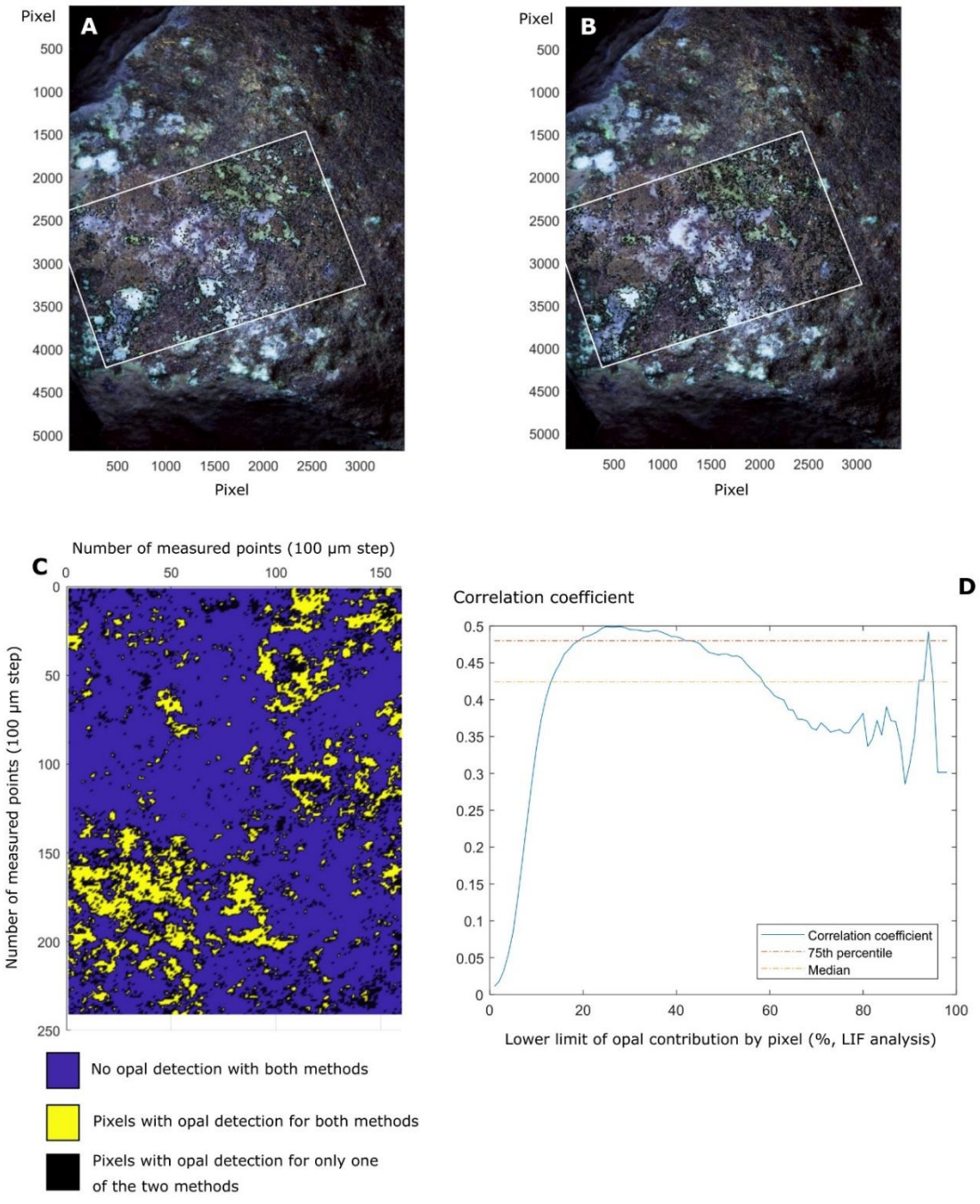

424

Figure 8*: Comparison of detection of opal mineralization on flake S-ECA-05 with UV illumination and UV LIF. A and B/ Photo under UV light and contour plot (black line) of opal presence calculated from the green component of the image (at least 8% of green) and from the MCR results (contribution of at least 25% of the total fluorescence) respectively for A and B, after geometric transformation (white square). C/ Cartography of pixels associated with the presence of opal comparing A and B (no*

geometric transformation). D/ Correlation coefficient between opal presence images obtained with the two methods (% of opal contribution correspond to lower boundaries applied for pixels selection).

425

426 *4.4.2 Visual detection under UV light: field experiments*

427

428 An *in situ* photographic protocol that alternated white light and UV illumination was applied to the
429 Points Cave walls. As shown in Figure 1, three rock art panels and one wall devoid of any rock art
430 were investigated. Pictures were taken at both the wall and macroscopic scales.

431

432 At the wall scale, the rock art panels investigated (Points Recess, Bi-lobed Signs and Ibexes) displayed
433 large green fluorescent zones when illuminated by UV LEDs (Figure 9). This green fluorescence
434 response was consistent with preliminary results obtained in the laboratory on cave wall flakes and µ-
435 samples from these zones. Thus, UV illumination successfully enabled the detection of opal coatings
436 on these walls, according to the green response observed in photographs.

437

438 In contrast, no opal signal appeared clearly distinguishable in photographs of the wall situated a few
439 metres before the art panel (S.I.7). These photographs displayed greenish fluorescence mixed with
440 other signals, making it difficult to identify and extract green colour with accuracy. Spectroscopic
441 measurements need to be performed to precisely identify the presence of opal.

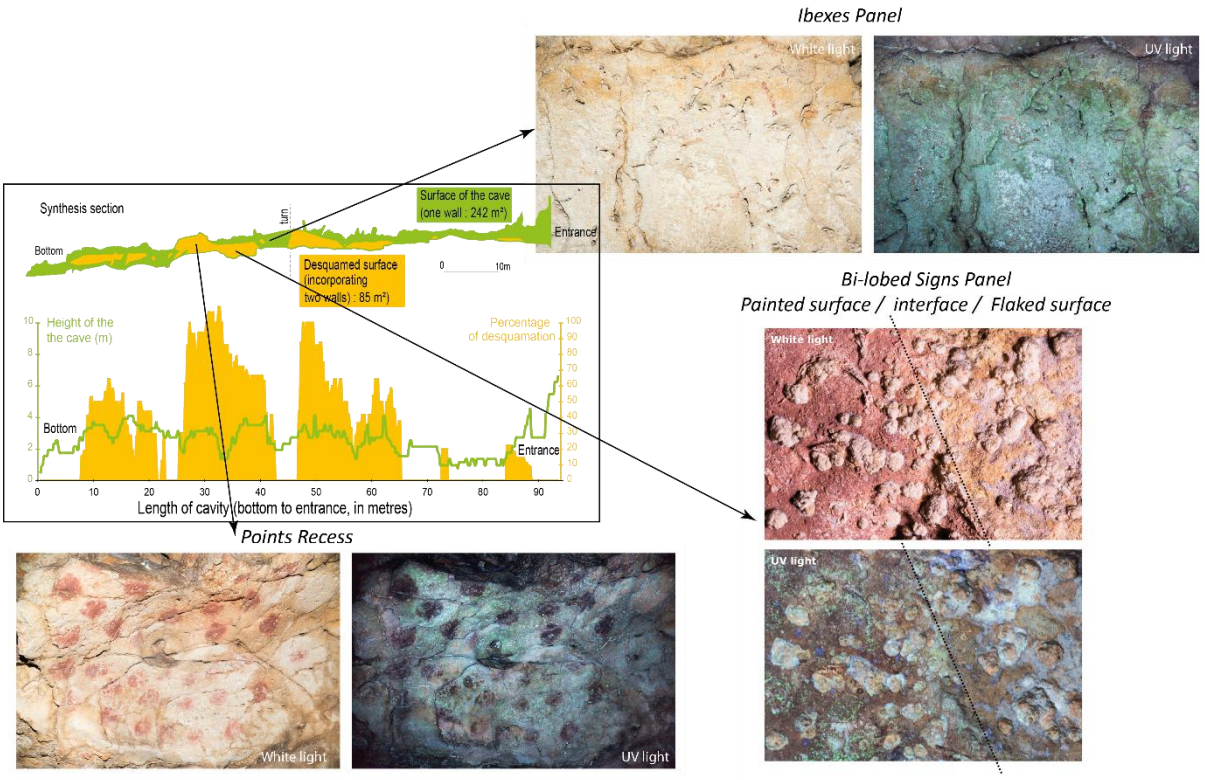

442

443 ***Figure 9**: Topographic section of Points Cave with estimated flaking rate of the cave walls according*

444 *to the distance to the entrance and location of white and UV light photographs according to Jaillet &*

445 *Monney, 2018.*

446

447 Macroscopic-scale observations under UV light allowed the targeting of specific deposits or zones on

448 cave walls. In the particular case of the Bi-lobed Signs panel, macroscopic investigation targeting

449 flaked zones revealed a contrast between the well-preserved rock art panels and the afterwards flaked

450 areas. Indeed, the painted surface of the UV photograph (left part of photograph, Figure 9) displayed

451 numerous green fluorescent spots, whereas they were absent from the right part of the photograph.

452 Efflorescence concretions on cave walls, which are widely spread in Points Cave, were also

453 investigated, but the presence of opal has not yet been validated.

454

455 **5. Discussion: Implications of opal detection for rock art studies at Points Cave**

456

5.1 Contribution of UV fluorescence techniques

According to the first results obtained using the *in situ* UV illumination method and the preliminary results obtained in the laboratory on cave wall flakes and µ-samples from rock art panels, *in situ* measurements successfully detected the presence of opal in Points cave. Indeed, the green fluorescence observed on Points Recess, Bi-lobed Signs and Ibexes panels suggests that opal development covers a large area of cave walls, especially in rock art sector. Macroscopic observations also help to provide initial insights into rock art-opal interactions, as UV light allows for the targeting of specific deposits or zones on cave walls. It provides complementary information on opal distribution and interaction with archaeological material. For example, investigation of the flaking zone suggests a current absence of extended opal film or opal mineralization, probably due to desquamation occurring on this wall.

However, the opal signal is not always clearly distinguishable, as observed on the wall outside of the rock art sector or on coralloid concretions. Yet, these speleothems are known to contain a silica layer enriched with uranium (Barbarand & Nouet, 2020). Alternating layers of silica and calcite or the presence of calcite cover could explain the ambiguous signal. First, this highlights the need for *in situ* fluorescence spectroscopic measurements to validate the photographic identification of the opal mineral phase in cases where the green response is not clearly detectable. Second, colour perception varies greatly from one image to another, even within the same site, making it difficult to evaluate the mineral phase distribution. Even if camera and image treatment parameters influencing colour display (white balance, exposure time, filters, etc.) can be easily standardized, lighting variations (LED orientation, position, distance from wall, etc.) are difficult to homogenize. As this paper presents preliminary results attempting to validate the detection method, no protocol for colour calibration was applied on UV photographs. Further research on the Points Cave site will be subject to the development of a colour calibration procedure.

Finally, UV illumination also highlights various types of deposits, sometimes not clearly detected under white light. After fluorescence analyses in the laboratory or directly *in situ*, this technique could help to detect other mineral or organic phases. Moreover, it is interesting to note that UV illumination emphasizes the presence of pigments due to their iron composition. Indeed, iron ions are known to have a quenching effect on the fluorescence signal, including that of uranyl ions (Backes, 2004; Gaillou *et al.*, 2008; Chen *et al.*, 2011). Thus, pigments appear clearly as no fluorescence zones on UV photographs, which can be an interesting tool for rock art analysis, such as determination of sampling protocol or dermatoglyph analysis.

UV methodology appears to be an efficient non-invasive tool for the *in situ* identification of U-silica mineralization, and of U-opal mineralization in this case. Due to the green fluorescence resulting from UV excitation, it allows rapid *in situ* detection of the opal mineral phase with direct results and very simple and low-cost equipment. As this method has already been applied with success in some caves, rarely calcareous, for the detection of U-silica complex deposits or concretions, as in Castañar Cave (Garcia-Guinea *et al.*, 2013), this study differs in two ways. First, to our knowledge, this method has never been applied to opal detection in a rock art context. Second, we propose *in situ* opal identification based on spectral features for result validation using a portable UV LIF instrument. This instrument is currently in development and could not yet be taken into the cave, but preliminary tests applied to flakes in the laboratory confirm its ability to detect opal. Finally, opal mineral characterization can also be achieved with high-spatial resolution at the microscopic scale with a laboratory UV LIF instrument. Spatially high-resolution fluorescence maps can also provide more information on mineral phase repartition, development and interaction with other organic and mineral phases present on the sample. Thus, the combination of these two methodologies provides a complete solution for the identification and detection of opal mineralization in both sampling and analytical strategies and *in situ* characterization.

5.2 What we know about Points Cave opal

The results obtained with the analyses presented in this paper and with UV methods applied to samples and *in situ* have provided the first information on opal coatings in Points Cave. Indeed, based on SEM analyses of flakes and µ-samples, Points Cave opal can be identified as the amorphous opal type (type A). XRD is usually performed for precise opal type determination (Curtis *et al.*, 2019). However, in the case of Points Cave opal, this analysis is difficult to perform due to the thinness of the opal layer and to the presence iron-rich pigments. Analyses at macro- and microscopic scales suggest thin film deposition as a mineralization type, such as silica skins observed at various rock art sites (Watchman, 1990; Green *et al.*, 2017). This film appears to be deposited under or at the interface with pigment and other crusts. SEM analyses show that the opal structure encapsulates hematite plates on several samples, suggesting strong interactions with pictorial matter (Figure 4). Further studies must be conducted to understand how these two phases interact, but a preliminary hypothesis regarding dissolution and corrosion of hematite plates by opal can be proposed.

The presence of uranyl ions entrapped in the opal structure was verified by UV spectroscopic analyses. High fluorescence intensities of opal at Points Cave suggest significant content of uranium trapped in the crystalline structure. Similar enrichment in uranium has been found in numerous common opals (Amelin & Back, 2006). However, at Points Cave, no quantification of uranium content has yet been realized. Although uranium isotopic measurements were realized on speleothems from Points Cave (stalagmites and coralloids), because of their destructive character, none was applied on flakes, or flake and wall µ-samples. According to the literature, as no minerals containing U^{4+} are known to fluoresce, uraniferous silica precipitation involves oxidizing conditions sufficient to mobilize U^{6+} (Zielinski, 1982). For example, Garcia-Guinea *et al.* (2013) explained uranium-bearing opal deposition in Castañar Cave by oxidation of host rocks with meteoritic waters. Zielinski (1982) explained that the initial precipitation of silica was as an amorphous silica gel, with which dissolved uranium coprecipitated before the silica gel dehydrated to form opal. The formation of uranyl-silica complexes is favoured by the natural affinity between aqueous uranyl ions and the silica gel surface,

538 which is very sensitive to pH (optimum range = pH 5-5.5) (Garcia-Guinea *et al.*, 2013).

539

540 The *in situ* approach shows an important spread of this coating on Points Cave walls, especially on
541 rock art panels. Concerning the undecorated walls a few metres away from the rock art sector, the
542 presence of opal needs to be confirmed by spectroscopic measurement and laboratory analyses. Points
543 Cave chronology is constrained by different periods marked by cave wall evolution under climatic and
544 anthropogenic factors (Monney & Jaillet, 2019). The presence of opal mineralization throughout its
545 formation and developmental processes could provide insights into cave chronology. A flaking period
546 was identified subsequent to the rock art phase, resulting from mechanical expansion or desquamation,
547 affecting the deepest zones of the cave, and possibly concurrent with gelifraction at the end of MIS2
548 (Marine Isotope Stage) and/or beginning of MIS1 (Monney & Jaillet, 2019). As described previously,
549 UV photographs indicated the absence of a well-developed opal film in the flaking zone, suggesting
550 that opal formation occurred principally before this flaking period. This could also explain why
551 photographs taken on walls between the cave angle and the rock art sectors displayed less marked
552 fluorescence, as this zone presents high flaking rates (Jaillet & Monney, 2018) (Figure 9).

553

554 The chronology of opal deposits over rock paintings and drawings cannot be confirmed at this stage.
555 SEM observations show that opal mineralization colonizes empty spaces above, below, and inside
556 pictorial matter. These observations suggest an opal deposition subsequent to painting realization,
557 although prior mineralization cannot be ruled out.

558

559 Thus, ongoing studies are crucial in completing opal coating characterization in Points Cave. This is a
560 tool in understanding cave wall and pigment interactions throughout the factors and processes of opal
561 formation and other mineralization.

562

563 *5.3 Opal factors and formation*

564

Mineralization origin and formation mechanisms and factors are clues for understanding past climate and cave wall evolution. As this paper presents preliminary results, only hypotheses for opal origin and formation are presented.

Opal, as a hydrated mineral, is associated with fluid circulation. Thus, water is generally involved in precipitation, and silica has to be in solution before precipitation (Chauviré *et al.*, 2017). In Points Cave, the presence of silica coating with high uranium content in the limestone context supports the hypothesis of mineralization originating from groundwater. Wall humidification and water physicochemical properties directly influence the coating formation rate. In very wet sites, the silica skin growth rate can reach 0.25 mm per millennia, whereas occasionally wet sites present a mineralization rate on the order of 0.02 mm per millennia (Aubert *et al.*, 2004). Silica coatings can only be formed and preserved if low infiltration volumes occur, as higher volumes favour dissolution of soluble compounds and decrease silica precipitation (Aubert *et al.*, 2004).

Chauviré *et al.* (2017) explained that even though opal is found in various geological contexts, three main types of formation can be identified: 1) hydrothermal activity, 2) biological precipitation and 3) continental weathering. As no hydrothermal activity was identified at Points Cave, only the latter two types can be involved in opal formation at this site.

Biological formation of opal in caves is less documented than hydrothermal alteration and continental weathering. Various microbial forms and algae have been observed to be associated with opal in caves, such as siliceous algal diatoms (Northup *et al.*, 2001), and are often linked to coralloid concretions. In the case of Points Cave, a few microscopic and cave wall µ-sample observations show undetermined structures containing high carbon content, which could be associated with biological activity. Nevertheless, the hypothesis of biological formation of opal cannot be ruled out or confirmed at this stage.

Continental weathering is defined by rock transformation by meteoric water and a precipitation temperature below 50°C, in contrast to hydrothermal alteration (Chauviré *et al.*, 2017). Silica anions released by this process precipitate because of fluid supersaturation due to various changes in conditions, such as pH or temperature (Devès *et al.*, 2012; Chauviré *et al.*, 2017). Thus, supersaturation of silica solutions may be initiated by a drop in temperature or pH, or an increase in salinity. When a solution is supersaturated in SiO_2, silicic acid could polymerize to form a colloidal suspension from which amorphous silica can precipitate. Polymerization is controlled by temperature (decreasing T° increases the polymerization rate), degree of supersaturation, salinity and mainly pH (maximum polymerization rate around pH 7.5; minimum polymerization rate under pH 3 and above 9) (Devès *et al.*, 2012). One of the most efficient pH-driven mechanisms for silica precipitation involves acidification of highly alkaline solutions (Zielinski, 1982). Such alkaline conditions are not common, but in the case of calcite-dominant material in sediment, pH could reach this threshold (Karkanas *et al.*, 1999). Freezing temperature has also been shown to help supersaturation, polymerization and rapid precipitation of opal, whereas low or moderate temperatures induce slow polymerization (months or years) (Devès *et al.*, 2012). Cryo-segregation is another reported genesis, caused by moisture freezing on cave walls, which concentrates dissolved salts. They precipitate out in the case of supersaturation of the solution (Devès *et al.*, 2012). As opal formation probably occurred during the Late Pleistocene possibly up until the Tardiglacial era and because freezing temperatures have been shown to have modified Points Cave wall topography, a temperature decrease represents a realistic factor for opal formation. However, there is currently a lack of evidence to confirm this hypothesis.

To help understand opal formation, the source of silica and uranium forming this mineralisation can also be questioned. Silica can originate from 1) superficial cover, 2) host rock, or 3) volcanic ash in a continental weathering context (Devès *et al.*, 2012). Volcanic ash is an interesting hypothesis, as it is assumed to provide both high contents of silica and uranium, and because the Ardèche region had recent volcanic episodes during the Upper Palaeolithic. Indeed, volcanic eruptions in the Bas-Vivarais region were dated between 23.9 ± 8.1 ka and 31.1 ± 3.9 ka (Nomade *et al.*, 2016; Sasco *et al.*, 2017).

619 The current alluvial plain and the lowest former alluvial level (+8 m) deposits contain much basaltic
620 material partly derived from Bas-Vivarais lava, which were subjected to intense erosion and
621 weathering in the alluvium terraces (Genuite *et al.*, 2021). Thus, the location and chronology of the
622 volcanic activity (approximately 45 km away from Points Cave) represent an interesting origin
623 hypothesis for both silica and uranium contents in opal. However, determining the origin of uranyl-
624 enriched silica solutions is difficult with our current information. Another hypothesis for silica
625 solution origin can be supported by the presence of a marl layer within the Urgonian limestone, which
626 constitutes the cave environment (Sadier, 2013); or by pebbles originating from former fluvial deposits
627 originated from the Ardèche River and providing silica by infiltration from the overlaying alluvium
628 terrace or by river deposition (Mocochain *et al.*, 2009; Tassy *et al.*, 2013; Genuite *et al.*, 2021).
629
630 Thus, understanding the origin and mineralization factors that influence opal formation could provide
631 information on chemical and physical processes occurring on the cave wall surface. According to
632 Green *et al.* (2017), this knowledge is "crucial for targeted sample collection and the application of a
633 range of dating techniques as well as for the development of conservation strategies".
634
635 *5.4 Chronology and dating*
636
637 Red pigments used in rock art are difficult to date precisely (Aubert *et al.*, 2007). Thus, several studies
638 have proposed indirect dating methods using associated mineral deposits interlaying pictorial matter to
639 date or to provide chronological constraints on rock paintings (Watchman, 1990; Aubert *et al.*, 2007;
640 Aubert *et al.*, 2017), such as opal coatings.
641
642 Indeed, in the first place, opal coating could help to precise relative chronology thanks to knowledge
643 regarding climatic and environmental factors controlling its mineralization, and to its distribution on
644 walls in comparison to other deposits and archaeological material.
645

Amorphous silica skins have been used for radiocarbon analyses based on organic remains trapped by mineralization, such as diatoms or algal matter, on different Australian rock art sites (Watchman, 2000; Morwood *et al.*, 2010). However, as silica coatings may contain various organic materials, each presenting a specific radiocarbon signature, dating could result in a mixture of different ages by incorporation of younger or older material (Aubert *et al.*, 2017; Green *et al.*, 2017). In addition, the formation processes of these coatings are not fully understood, requiring great caution when using radiocarbon methods (Aubert *et al.*, 2017). Using compound-specific carbon analyses could potentially avoid this problem (Aubert *et al.*, 2017) but are more difficult to apply to thin deposits, especially in rock art contexts.

Moreover, opal often contains high uranium contents, which could be used for high-precision dating with methods such as ^{230}U/Th or U/Pb (Zielinski, 1980; Oster *et al.*, 2017). Because of opal's ability to concentrate uranium from water while rejecting Pb and Th, amorphous silica is an interesting alternative to carbonate minerals (Amelin & Back, 2006). Indeed, ^{230}Th/U and U/Pb methods have been applied to opal and have provided reliable ages (Neymark & Paces, 2013). They enable chronological constraints or dating hydrogenic subsurface water flow, pedogenesis, and processes such as ore formation deposits (Neymark & Paces, 2013). They also have been applied in the case of paleoclimate reconstruction in silica speleothem studies (Lundberg *et al.*, 2010). Depending on the formation processes, opal coating could thus be used for dating purposes.

In rock art research, dating of amorphous silica deposits could be used as an age constraint for rock drawing events, depending on the pigments and mineral phase superimposition. In their study, Aubert *et al.* (2007) performed U-series dating on a 2.5 mm thick calcite coating using the MC-ICPMS technique, allowing high spatial and temporal resolution. Even though only micrograms of samples are needed, authors (Aubert *et al.*, 2007; Aubert *et al.*, 2017) have suggested that for samples with U concentrations > 1 ppm, sampling could be largely reduced, and LIBS techniques could also be applied *in situ* with a 100-200 µm diameter ablation spot. As opal concentrates more U than calcite,

these techniques appear to be possible. However, for some authors, the application of uranium series dating to silica skins appears difficult to achieve (Green *et al.*, 2017). Sampling that provides sufficient intact fragments for LA-ICP-MS analysis without damaging rock paintings is one of the main issues regarding this application. The difficulty of performing closed system conditions and replicability tests for evaluating dating reliability has also been highlighted by authors.

Moreover, methods for opal detection could offer supplemental help before sampling for dating. Indeed, precise targeting of uranium-bearing opal enables identification of pure silica phases in mixed samples, detection of high uranium contents or impurity avoidance. In the case of thin layer deposits, such as in coralloids, sampling could decrease dating accuracy when mixing different layers (Devès *et al.*, 2012). Tracking the location of opal phases could avoid this issue by spatially constraining sampling.

5.5 Implication of opal mineral characterization for conservation of rock art material

Taphonomy represents a range of transformations affecting archaeological material that distort archaeological records. Thus, rock paintings have undergone a plurality of transformations impacting pigment longevity, colour and identification (Bednarik, 1994; Huntley, 2012; Chalmin *et al.*, 2018; Rousaki *et al.*, 2018; Defrasne *et al.*, 2019). At Points Cave, the extensive presence of dermatoglyphs on 47 palm prints is exceptional (Achtelik *et al.*, 2019). In fact, to our knowledge, it has no equivalent in European Palaeolithic cave art which raises the question of opal impact on pigment conservation.

If pigment weathering can be influenced by their own properties by inducing changes in surface area, albedo, light transmissivity or moisture (Huntley, 2012), mineral deposits have been recognized to be important factors in rock art taphonomy (Chalmin *et al.*, 2018). In addition to analytical impacts, knowledge of mineral phases is essential because it informs us regarding the physical and chemical impacts on pictorial matter and whether they favour conservation or degradation effects. Mineral

phase characterization is thus an important part of conservation strategies, and adapted identification and analytical methods are needed.

The association of silica skins composed of opal and pigments has been frequently observed at rock art sites, mainly in open-air sites on sandstone and quartzite substrates in Australia or Canada (Watchman, 1990; Aubert *et al.*, 2004; Aubert *et al.*, 2012; Huntley, 2012). Some studies have suggested that pigment binding in silica coatings aids rock art visual preservation (Watchman, 1990), providing a resistant layer to chemical weathering. SEM observations on Points Cave flake and wall µ-samples indeed suggest a strong interaction between pigments and opal, as mineralization penetrates pigment deposits. If the quality of Points Cave paintings tends to corroborate this hypothesis, exfoliation impacting silica skins observed at some sites should also be mentioned, as it could cause removal of associated pigments (Aubert *et al.*, 2004; Green *et al.*, 2017). Thus, exploiting the observed benefits of silica film deposits for conservation strategies has not yet been proven (Green *et al.*, 2017). Furthermore, it has also been observed at open-air sites that silica skins could reduce the colour tone of paintings and drawings at some locations (Green *et al.*, 2017).

6. Conclusion

The methodological development proposed in this paper was motivated by the presence of opal in cave art context at Points Cave. Its identification *in situ*, in the laboratory, on centimetric objects and on µ-samples questions the possibility of accessing the specificities of the colouring matter applied on the walls (petrography and geochemistry). Therefore, *in situ* identification of silica coating observed in the laboratory was crucial for further studies on pigment characterization.

The results obtained on flakes and flake µ-samples from Points Cave show that UV LIF is an efficient technique to detect and identify uranyl-silica complexes, even on heterogeneous and complex surfaces.

Although opal coating detection is limited by the outcropping nature of the deposit, UV LIF spectroscopy offers a rapid and non-invasive tool that can easily be brought to the site and positioned in front of the rock art panels. A photograph of green bright fluorescence emitted by opal was used here as a method for *in situ* detection of this mineral coating. A comparison with the UV LIF method shows a great correspondence between the two methods. The first tests of UV illumination in the cave highlight the need to develop an accurate measurement protocol, especially to homogenize light and colour, and the need to validate the identification using UV LIF spectroscopy. In addition to further methodological development, UV optical technique shows great potential because it successfully detects the presence of opal and its distribution on rock art panels.

The results obtained with our methodology provide insights into disturbances in the classical *in situ* spectroscopic analyses (pXRF) observed at Points Cave (Chanteraud *et al.*, 2021). The identification and characterization of opal coating is thus essential because its impact on *in situ* analysis could disturb the detection of iron-oxide spectroscopic signal in case of Raman analysis for example. For this reason, we propose early, on-site observations combined with sampling of surrounding material, such as fallen flakes from cave walls, as an alternative strategy to i) characterize pigment-associated mineral phases, ii) choose the best site-adapted combination of techniques and devices for *in situ* analyses and iii) define laboratory analytical strategies depending on the pictorial matter environment. Moreover, optical methods with *in situ* visual detection, such as the UV light illumination method proposed in this paper, represent an interesting tool to add to sampling and analytical strategies. Visualization at a larger scale of the presence and distribution of mineral deposits that could interfere with pigment analyses is a great help in locating sampling or *in situ* measurements to avoid interference.

In addition to analytical impacts, the detection and identification of mineral phases can provide valuable information on the pigment environment and human practice chronology. If speleothems are considered an accurate archive for past climate and environment, other mineral deposits could provide

753 informative records on the setting and evolution of archaeological evidence. Applying a specific
754 methodology for their characterization is thus an efficient tool in improving rock art knowledge.
755
756 Thanks to opal mineralization detection utilizing UV methodologies on cave walls, a discussion on its
757 formation and associated factors, such as climatic, hydrologic or geomorphologic conditions over time
758 can be started. Thus, the mineral form described as opal can provide elements on cave natural history.
759

760 **Acknowledgements**

761

762 We would like to thank Frédérique Charlot, microscopist at CMTC (INPE, Grenoble).
763 Funding was provided by ANR LabCom SpecSolE, DRAC Occitanie, DRAC AURA
764 (Pigmentothèque project), French Ministry of Culture and University Savoie Mont Blanc.
765

766 **Conflict of interest disclosure**

767 The authors declare they have no conflict of interest relating to the content of this article.
768

769 **Data, script and code availability**

770 *S.I.1. Macroscopic pictures and SEM data of flakes µ-samples:*

771 https://doi.org/10.6084/m9.figshare.16832593.v2

772 https://doi.org/10.6084/m9.figshare.16832557.v3

773 https://doi.org/10.6084/m9.figshare.16832452

774 https://doi.org/10.6084/m9.figshare.16832605

775

776 *S.I.2. Macroscopic pictures and SEM data of rock art µ-samples:*

777 *https://doi.org/10.6084/m9.figshare.19142243.v1*

https://doi.org/10.6084/m9.figshare.19142267.v1

https://doi.org/10.6084/m9.figshare.19142276.v1

https://doi.org/10.6084/m9.figshare.19142300.v1

https://doi.org/10.6084/m9.figshare.19142351.v1

https://doi.org/10.6084/m9.figshare.19142354.v1

https://doi.org/10.6084/m9.figshare.19142366.v1

https://doi.org/10.6084/m9.figshare.19142372.v1

https://doi.org/10.6084/m9.figshare.19142375.v1

https://doi.org/10.6084/m9.figshare.19142381.v1

https://doi.org/10.6084/m9.figshare.19142384.v1

https://doi.org/10.6084/m9.figshare.19142387.v1

S.I.3. Single UV fluorescence measurement (raw data):

https://doi.org/10.6084/m9.figshare.16837180.v1

S.I.4. UV fluorescence cartography measurement (raw data):

https://doi.org/10.6084/m9.figshare.16837324.v3

S.I.5. UV fluorescence data processing (Matlab script):

https://doi.org/10.6084/m9.figshare.16837405.v2

S.I.6. pXRF result of in situ analysis at the Points Cave:

https://doi.org/10.6084/m9.figshare.9791405.v1

https://doi.org/10.6084/m9.figshare.9791210.v1

803 *S.I.7. In situ UV photographs*

804 *https://doi.org/10.6084/m9.figshare.19316588.v1*

805

806 **Bibliography**

807 Achtelik M., Floss H., Nagel M., Monney, J., 2019. Analyse chiroscopique des points-paumes de la
808 grotte aux Points (Aiguèze, Gard). *Karstologia* 73, pp 33-40.

809

810 Amelin, Y., Back, M., 2006. Opal as a U–Pb geochronometer: search for a standard. *Chemical*
811 *Geology* 232, 67–86. https://doi.org/10.1016/j.chemgeo.2006.02.018

812

813 Araya, J.A., Carneiro, R.L., Arévalo, C., Freer, J., Castillo, R. del P., 2017. Single pixel quantification
814 strategies using middle infrared hyperspectral imaging of lignocellulosic fibers and MCR-ALS
815 analysis. *Microchemical Journal* 134, 164–172. https://doi.org/10.1016/j.microc.2017.05.019

816

817 Aubert, M., 2012. A review of rock art dating in the Kimberley, Western Australia. *Journal of*
818 *Archaeological Science* 39, 573–577. https://doi.org/10.1016/j.jas.2011.11.009

819

820 Aubert, M., Watchman, A., Arsenault, D., Gagnon, L., 2004. L'archéologie rupestre du Bouclier
821 canadien : Potentiel archéométrique. *Canadian Journal of Archaeology/Journal Canadien*
822 *d'Archéologie* 51–74. http://www.jstor.org/stable/41103470

823

824 Aubert, M., O'Connor, S., McCulloch, M., Mortimer, G., Watchman, A., Richer-LaFlèche, M., 2007.
825 Uranium-series dating rock art in East Timor. *Journal of Archaeological Science* 34, 991–996.
826 https://doi.org/10.1016/j.jas.2006.09.017

827

828 Aubert, M., Brumm, A., Taçon, P.S., 2017. The timing and nature of human colonization of Southeast

Asia in the late Pleistocene: A rock art perspective. *Current Anthropology* 58, S553–S566. https://doi.org/10.1086/694414

Backes, C. J., 2004. More Than Meets the Eye: Fluorescence Photography for Enhanced Analysis of Pictographs. *Journal of California and Great Basin Anthropology*, 24(2), 193–206. http://www.jstor.org/stable/27825774

Barbarand, J., Nouet, J., 2020. Pétrographie et minéralogie des coralloïdes de la grotte au Points, in: Monney J. (Dir.). Projet Datation Grottes Ornées : Rapport d'activité 2020. Grotte Aux Points (Aiguèze). Rapport Non Publié., Ministère de La Culture, SRA Occitanie, Montpellier.

Bassel, L., 2017. Genèse de faciès calcitiques : mondmilch et coralloïdes. Étude multiphysique des concrétions de la grotte laboratoire de Leye (Dordogne) (Thèse). Université Bordeaux Montaigne. https://tel.archives-ouvertes.fr/tel-01729035

Bednarik, R.G., 1994. A taphonomy of palaeoart. *Antiquity* 68, 68–74. https://doi.org/10.1017/S0003598X00046202

Boyko, V., Dovbeshko, G., Fesenko, O., Gorelik, V., Moiseyenko, V., Romanyuk, V., others, 2011. New optical properties of synthetic opals infiltrated by DNA. *Molecular Crystals and Liquid Crystals* 535 (1), 30-41. https://doi.org/10.1080/15421406.2011.537888

Brennan, E. S., White, W. B., 2013. Luminescence of speleothems: a comparison of sources and environments. *Journal of Cave & Karst Studies*, 75(3).

Castro, R.C., Ribeiro, D.S., Santos, J.L., Páscoa, R.N., 2021. Near infrared spectroscopy coupled to MCR-ALS for the identification and quantification of saffron adulterants: Application to complex

mixtures. Food Control 123, 107776. https://doi.org/10.1016/j.foodcont.2020.107776

Chalmin, E., Hoerlé, S.H., Reiche, I., 2018. Taphonomy on the Surface of the Rock Wall: Rock-Paint-Atmosphere Interactions. Bruno David; Ian J. McNiven. The Oxford Handbook of the Archaeology and Anthropology of Rock Art, Oxford Handbook. https://hal.archives-ouvertes.fr/hal-01801656/

Chalmin, E., Salomon, H., Chassin de Kergommeaux, A., Chanteraud, C., 2019. Construction d'une Pigmentothèque : un outil pour comprendre l'approvisionnement en matériaux colorants durant la Préhistoire : Rapport d'activité 2019. [Rapport de recherche] DRAC/SRA; Auvergne Rhône Alpes. 2019. ⟨hal-02429867⟩

Chanteraud, C., 2020. Matières colorantes et grottes ornées des gorges de l'Ardèche. Méthodes d'analyse des ressources et liens culturels au Paléolithique supérieur : application à la grotte aux Points (Aiguèze, Gard, France) (Thèse). Université Savoie Mont Blanc. https://tel.archives-ouvertes.fr/tel-03184877

Chanteraud, C., Chalmin, E., Hoerlé, S., Salomon, H., Monney, J., 2019. Relation entre les matières colorantes issues des fouilles et des parois ornées. Méthodologie et première perspective comparative à la Grotte aux Points (Aiguèze, Gard, France). *Karstologia* 73, pp 1-12. https://hal.archives-ouvertes.fr/hal-01756858/

Chanteraud, C, Chalmin, É., Lebon, M., Salomon, H., Jacq, K., Noûs, C., Delannoy, J.-J., Monney, J. 2021. Contribution and limits of portable X-ray fluorescence for studying Palaeolithic rock art: a case study at the Points cave (Aiguèze, Gard, France). *Journal of Archaeological Science: Reports* 37: 102898. https://doi.org/10.1016/j.jasrep.2021.102898

Chauviré, B., Rondeau, B., Mangold, N., 2017. Near infrared signature of opal and chalcedony as a

proxy for their structure and formation conditions. European Journal of Mineralogy 29, 409–421. https://doi.org/10.1127/ejm/2017/0029-2614

Chen, C.-C., Pestov, D., Nelson, J.D., Anderson J.E. and G. Tepper, 2011. Uranyl Soil Extraction and Fluorescence Enhancement by Nanoporous Silica Gel: pH effects. J Fluoresc 21, 119–124. https://doi.org/10.1007/s10895-010-0695-0

Curtis, N.J., Gascooke, J.R., Johnston, M.R., Pring, A., 2019. A review of the classification of opal with reference to recent new localities. Minerals 9, 299. https://doi.org/10.3390/min9050299

De Juan, A., Jaumot, J., Tauler, R., 2014. Multivariate Curve Resolution (MCR). Solving the mixture analysis problem. Analytical Methods 6, 4964–4976. https://doi.org/10.1039/C4AY00571F

Defrasne, C., Chalmin, E., Bellot-Gurlet, L., Thirault, E., and G. André, 2019. From archeological layers to schematic rock art? Integrated study of the Neolithic pigments and pigmented rocks at the Rocher du Château (Western Alps, Savoie, France). Archaeol Anthropol Sci 11, 6065–6091. https://doi.org/10.1007/s12520-019-00882-9

Delvigne, Jean E. 1998. *Atlas of Micromorphology of Mineral Alteration and Weathering*. The Canadian Mineralogist 3. Ottawa: Paris: Mineralogical Association of Canada; ORSTOM.

DeNeufville, J., Kasdan, A., Chimenti, R., 1981. Selective detection of uranium by laser-induced fluorescence: a potential remote-sensing technique. 1: Optical characteristics of uranyl geologic targets. Applied Optics 20, 1279–1296. https://doi.org/10.1364/AO.20.001279

908 Deschamps, E.B., Chauvet, J.M., Hillaire, C., 2018. La grotte aux Points d'Aiguèze : récits de
909 découverte d'une ornementation pariétale. Karstologia 72, 13–14.
910
911 Devès, G., Perroux, A.-S., Bacquart, T., Plaisir, C., Rose, J., Jaillet, S., Ghaleb, B., Ortega, R., Maire,
912 R., 2012. Chemical element imaging for speleothem geochemistry: Application to a uranium-bearing
913 corallite with aragonite diagenesis to opal (Eastern Siberia, Russia). Chemical Geology 294, 190–202.
914 https://doi.org/10.1016/j.chemgeo.2011.12.003
915
916 Flörke, O., Graetsch, H., Röller, K., Martin, B., Wirth, R., 1991. Nomenclature of micro-and non-
917 crystalline silica minerals. Neues Jahrbuch für Mineralogie, Abhandlungen 163, 19–42.
918
919 Fritsch, E., Mihut, L., Baibarac, M., Baltog, I., Ostrooumov, M., Lefrant, S., Wery, J., 2001.
920 Luminescence of oxidized porous silicon: Surface-induced emissions from disordered silica micro-to
921 nanotextures. Journal of Applied Physics 90, 4777–4782. https://doi.org/10.1063/1.1410887
922
923 Fritsch, E., Wéry, J., Jonusauskas, G., Faulques, E., 2003. Transient photoluminescence from highly
924 disordered silica-rich natural phases with and without nanostructures. Physics and chemistry of
925 minerals 30, 393–400. https://doi.org/10.1007/s00269-003-0329-z
926
927 Fritsch, E., Megaw, P.K., Spano, T.L., Chauviré, B., Rondeau, B., Gray, M., Hainschwang, T., Renfro,
928 N., 2015. Green-luminescing hyalite opal from Zacatecas, Mexico. J. Gemmol 34, 490–508.
929
930 Gaillou, E., Delaunay, A., Rondeau, B., Bouhnik-le-Coz, M., Fritsch, E., Cornen, G., Monnier, C.,
931 2008. The geochemistry of gem opals as evidence of their origin. Ore Geology Reviews 34, 113–126.
932 https://doi.org/10.1016/j.oregeorev.2007.07.004
933
934 Garcia-Guinea, J., Fernandez-Cortes, A., Alvarez-Gallego, M., García-Antón, E., Casas-Ruiz, M.,

935 Blázquez-Pérez, D., Teijón, O., Cuezva, S., Correcher, V., Sanchez-Moral, S., 2013. Leaching of
936 uranyl–silica complexes from the host metapelite rock favoring high radon activity of subsoil air: case
937 of Castañar cave (Spain). Journal of Radioanalytical and Nuclear Chemistry 298, 1567–1585.
938 https://doi.org/10.1007/s10967-013-2587-7
939
940 Genuite, K., Delannoy, JJ., Bahain, JJ., Gresse M., Jaillet S., Philippe A., Pons-Branchu E., Revil A.,
941 and P. Voinchet, 2021. Dating the landscape evolution around the Chauvet-Pont d'Arc cave. Sci
942 Rep 11, 8944. https://doi.org/10.1038/s41598-021-88240-5
943
944 Gorobets, B., Engoyan, S., Sidorenko, G., 1977. Investigation of uranium and uranium-containing
945 minerals by their luminescence spectra. Soviet Atomic Energy 42, 196–202.
946 https://doi.org/10.1007/BF01121388
947
948 Green, H., Gleadow, A., Finch, D., Hergt, J., Ouzman, S., 2017. Mineral deposition systems at rock art
949 sites, Kimberley, Northern Australia—Field observations. Journal of Archaeological Science: Reports
950 14, 340–352. https://doi.org/10.1016/j.jasrep.2017.06.009
951
952 Huntley, J., 2012. Taphonomy or painT recipe: In situ portable x-ray fluorescence analysis of two
953 anthropomorphic motifs from the Woronora Plateau, New South Wales. Australian Archaeology 75,
954 78–94. https://doi.org/10.1080/03122417.2012.11681952
955
956 Huntley, J., Aubert, M., Ross, J., Brand, H. E., Morwood, M. J., 2015. One colour, (at least) two
957 minerals: a study of mulberry rock art pigment and a mulberry pigment 'quarry' from the Kimberley,
958 northern Australia. Archaeometry 57 (1), 77-99. https://doi.org/10.1111/arcm.12073

959

960 Jaillet, S., Monney, J., 2018. Analyse 3D des volumes et remplissages souterrains de la grotte aux
961 Points au temps des fréquentations paléolithiques (Aiguèze, Gard). Karstologia 72, 27–36.
962 https://hal.archives-ouvertes.fr/hal-01878453/

963

964 Jaumot, J., Gargallo, R., de Juan, A., Tauler, R., 2005. A graphical user-friendly interface for MCR-
965 ALS: a new tool for multivariate curve resolution in MATLAB. Chemometrics and intelligent
966 laboratory systems 76, 101–110. https://doi.org/10.1016/j.chemolab.2004.12.007

967

968 Jaumot, J., de Juan, A., Tauler, R., 2015. MCR-ALS GUI 2.0: New features and applications.
969 Chemometrics and Intelligent Laboratory Systems 140, 1–12.
970 https://doi.org/10.1016/j.chemolab.2014.10.003

971

972 Karkanas, P., Kyparissi-Apostolika, N., Bar-Yosef, O., Weiner, S., 1999. Mineral assemblages in
973 Theopetra, Greece: a framework for understanding diagenesis in a prehistoric cave. Journal of
974 Archaeological Science 26, 1171–1180. https://doi.org/10.1006/jasc.1998.0354

975

976 Kasdan, A., Chimenti, R.J.L., deNeufville, J.P., 1981. Selective detection of uranium by laser-induced
977 fluorescence: a potential remote-sensing technique. 2: Experimental assessment of the remote sensing
978 of uranyl geologic targets. Appl. Opt. 20, 1297–1307. https://doi.org/10.1364/AO.20.001297

979

980 Kinnunen, K.A., Ikonen, L., 1991. Opal, a new hydromorphic precipitate type from gravel deposits in
981 southern Finland. Bulletin of the Geological Society of Finland 63, 95–104.

982

Kumar, K., 2018. Application of Genetic Algorithm (GA) Assisted Partial Least Square (PLS) Analysis on Trilinear and Non-trilinear Fluorescence Data Sets to Quantify the Fluorophores in Multifluorophoric Mixtures: Improving Quantification Accuracy of Fluorimetric Estimations of Dilute Aqueous Mixtures. Journal of fluorescence 28, 589–596. https://doi.org/10.1007/s10895-018-2221-8

Lafon D., Konik S., Monney J. 2022. On-site spectroradiometric analysis of palaeolithic cave art: Investigating colour variability of red rock art at Points cave (Aiguèze, Gard, France). *Journal of Archaeological Science – report* 42, 103384. https://doi.org/10.1016/j.jasrep.2022.103384

Lundberg, J., Brewer-Carias, C., and D., McFarlane, 2010. Preliminary results from U-Th dating of glacial-interglacial deposition cycles in a silica speleothem from Venezuela. Quaternary Research, 74 (1), 113-120. https://doi.org/10.1016/j.yqres.2010.03.005

Mas, S., de Juan, A., Tauler, R., Olivieri, A.C., Escandar, G.M., 2010. Application of chemometric methods to environmental analysis of organic pollutants: a review. Talanta 80, 1052–1067. https://doi.org/10.1016/j.talanta.2009.09.044

Mauran, G., Lebon, M., Détroit, F., Caron, B., Nankela, A., Pleurdeau, D., Bahain, J.-J. 2019. First in Situ PXRF Analyses of Rock Paintings in Erongo, Namibia: Results, Current Limits, and Prospects. *Archaeological and Anthropological Sciences* 11 (8): 4123–45. https://doi.org/10.1007/s12520-019-00787-7

McGarry, S. F., Baker, A., 2000. Organic acid fluorescence: applications to speleothem palaeoenvironmental reconstruction. Quaternary Science Reviews 19(11), 1087-1101. https://doi.org/10.1016/S0277-3791(99)00087-6

Mocochain L., Audra, P., Clauzon, G., Bellier, O., Bigot, J.-Y., Parize, O., and P. Monteil, 2021. The

1010 effect of river dynamics induced by the Messinian Salinity Crisis on karst landscape and caves:
1011 Example of the Lower Ardèche river (mid Rhône valley), Geomorphology, 106 (1–2), 46-61.
1012 https://doi.org/10.1016/j.geomorph.2008.09.021.
1013
1014 Monger, H.C., Kelly, E.F., 2002. Silica minerals. Soil mineralogy with environmental applications 7,
1015 611–636.
1016
1017 Monney, J., 2011. Projet Datation Grottes Ornées : Rapport d'activité 2011. Grotte aux Points
1018 (Aiguèze). Rapport non publié, Ministère de la Culture, SRA Occitanie, Montpellier.
1019
1020 Monney, J., 2018. L'art pariétal paléolithique de la grotte aux Points d'Aiguèze: définition d'un
1021 dispositif pariétal singulier et discussion de ses implications. Karstologia 72, 45–60.
1022
1023 Monney, J. 2019. Projet Datation Grottes Ornées : Rapport 2019 (12ème volet) : 12.1. Grotte aux
1024 Points (Aiguèze). [Rapport de recherche] Ministère de la Culture, SRA Occitanie, Montpellier. 2019.
1025 ⟨hal-01972949⟩
1026
1027 Monney, J., Jaillet, S., 2019. Phases de fréquentations humaines, ornementation pariétale et processus
1028 naturels : Mise en place d'un cadre chronologique pour la grotte aux Points d'Aiguèze. Karstologia 72,
1029 49–62. https://hal.archives-ouvertes.fr/hal-01957634/
1030
1031 Morwood, M.J., Walsh, G.L., Watchman, A.L., 2010. AMS radiocarbon ages for beeswax and
1032 charcoal pigments in north Kimberley rock art. Rock Art Research: The Journal of the Australian
1033 Rock Art Research Association (AURA) 27 (1), 3–8.
1034 *https://search.informit.org/doi/10.3316/informit.153070840500133*
1035
1036 Neymark, L., Paces, J.B., 2013. Ion-probe U–Pb dating of authigenic and detrital opal from Neogene-

1037 Quaternary alluvium. Earth and Planetary Science Letters 361, 98–109.
1038 https://doi.org/10.1016/j.epsl.2012.11.037
1039
1040 Neymark, L.A., Amelin, Y.V., Paces, J.B., 2000. 206Pb–230Th–234U–238U and 207Pb–235U
1041 geochronology of Quaternary opal, Yucca Mountain, Nevada. Geochimica et Cosmochimica Acta 64,
1042 2913–2928. https://doi.org/10.1016/S0016-7037(00)00408-7
1043
1044 Nomade, S., Genty, D., Sasco, R., Scao, V., Féruglio, V., Baffier, D., Guillou, H., Bourdier, C.,
1045 Valladas, H., Reigner, E., others, 2016. A 36,000-year-old volcanic eruption depicted in the Chauvet-
1046 Pont d'Arc Cave (Ardèche, France)? PloS one 11(1), e0146621.
1047 https://doi.org/10.1371/journal.pone.0146621
1048
1049 Northup, K.H., Diana, Lavoie, 2001. Geomicrobiology of caves: a review. Geomicrobiology journal
1050 18, 199–222.
1051
1052 Oster, J.L., Kitajima, K., Valley, J.W., Rogers, B., Maher, K., 2017. An evaluation of paired δ18O and
1053 (234U/238U) 0 in opal as a tool for paleoclimate reconstruction in semi-arid environments. Chemical
1054 Geology 449, 236–252. https://doi.org/10.1016/j.chemgeo.2016.12.009
1055
1056 Othmane, G., Allard, T., Vercouter, T., Morin, G., Fayek, M., Calas, G., 2016. Luminescence of
1057 uranium-bearing opals: Origin and use as a pH record. Chemical Geology 423, 1–6.
1058 https://doi.org/10.1016/j.chemgeo.2015.12.010
1059
1060 Perrette, Y., Delannoy, J.-J., Bolvin, H., Cordonnier, M., Destombes, J.-L., Zhilinskaya, E.A.,

Aboukais, A., 2000. Comparative study of a stalagmite sample by stratigraphy, laser induced fluorescence spectroscopy, EPR spectrometry and reflectance imaging. Chemical Geology 162, 221–243. https://doi.org/10.1016/S0009-2541(99)00069-8

Perrette, Y., Delannoy, J. J., Desmet, M., Lignier, V., Destombes, J. L., 2005. Speleothem organic matter content imaging. The use of a Fluorescence Index to characterise the maximum emission wavelength. Chemical Geology 214 (3-4), 193-208. https://doi.org/10.1016/j.chemgeo.2004.09.002

Pons-Branchu, E., Bourrillon, R., Conkey, M.W., Fontugne, M., Fritz, C., Gárate, D., Quiles, A., Rivero, O., Sauvet, G., Tosello, G., 2014. Uranium-series dating of carbonate formations overlying Paleolithic art: interest and limitations. Bulletin de la Société préhistorique française 211–224. http://www.jstor.org/stable/24364541

Quiers, M., Perrette, Y., Chalmin, E., Fanget, B., Poulenard, J., 2015. Geochemical mapping of organic carbon in stalagmites using liquid-phase and solid-phase fluorescence. Chemical Geology 411, 240-247. https://doi.org/10.1016/j.chemgeo.2015.07.012

Quiles, A., Fritz, C., Alcaide, M.Á.M., Pons-Branchu, E., Torti, J.L.S., Tosello, G., Valladas, H., 2015. Chronologies croisées (C-14 et U/Th) pour l'étude de l'art préhistorique dans la grotte de Nerja: méthodologie. Presented at the Sobre rocas y huesos: las sociedades prehistóricas y sus manifestaciones plásticas, UCO Press. Editorial de la Universidad de Córdoba, pp. 420–427.

Rousaki, A., Vargas, E., Vázquez, C., Aldazábal, V., Bellelli, C., Calatayud, M. C., Hajduk A., Palacios O., Moens L., and P. Vandenabeele, 2018. On-field Raman spectroscopy of Patagonian prehistoric rock art: Pigments, alteration products and substrata. TrAC Trends in Analytical Chemistry, 105, 338-351. https://doi.org/10.1016/j.trac.2018.05.011

1088 Sadier, B., 2013. 3D et géomorphologie karstique : La grotte Chauvet et les cavités des Gorges de
1089 l'Ardèche (Thèse). Université de Savoie, Le-Bourget-Du-Lac. https://hal.univ-smb.fr/tel-01070711/
1090
1091 Salomon, Hélène, Claire Chanteraud, Aurélie Chassin de Kergommeaux, Julien Monney, Jean-Victor
1092 Pradeau, Éric Goemaere, Yvan Coquinot, and Emilie Chalmin. 2021. 'A Geological Collection and
1093 Methodology for Tracing the Provenance of Palaeolithic Colouring Materials'. *Journal of Lithic*
1094 *Studies* 8 (1): 38-p. https://doi.org/10.2218/jls.5540
1095
1096 Sasco, R., Guillou, H., Nomade, S., Scao, V., Maury, R. C., Kissel, C., & Wandres, C., 2017.
1097 40Ar/39Ar and unspiked 40K-40Ar dating of upper Pleistocene volcanic activity in the Bas-Vivarais
1098 (Ardèche, France). Journal of Volcanology and Geothermal Research, 341, 301-314.
1099 https://doi.org/10.1016/j.jvolgeores.2017.06.003
1100
1101 Savitzky, A., Golay, M.J.E., 1964. Smoothing and Differentiation of Data by Simplified Least Squares
1102 Procedures. Analytical Chemistry. 36, 1627–1639. https://doi.org/10.1021/ac60214a047
1103
1104 Shao, Q.-F., Pons-Branchu, E., Zhu, Q.-P., Wang, W., Valladas, H., Fontugne, M., 2017. High
1105 precision U/Th dating of the rock paintings at Mt. Huashan, Guangxi, southern China. Quaternary
1106 Research 88, 1–13. https://doi.org/10.1017/qua.2017.24
1107
1108 Tassy, A., Mocochain, L., Bellier, O., Braucher, R., Gattacceca, J., & Bourlès, D., 2013. Coupling
1109 cosmogenic dating and magnetostratigraphy to constrain the chronological evolution of peri-
1110 Mediterranean karsts during the Messinian and the Pliocene: Example of Ardèche Valley, Southern
1111 France. Geomorphology, 189, 81-92. https://doi.org/10.1016/j.geomorph.2013.01.019
1112

1113 Trosseau, Antoine, Anne Maigret, Yvan Coquinot, and Ina Reiche, 2021. In Situ XRF Study of Black
1114 Colouring Matter of the Palaeolithic Figures in the Font-de-Gaume Cave. *Journal of Analytical Atomic*
1115 *Spectrometry* 36 (11): 2449–59. https://doi.org/10.1039/D1JA00202C
1116
1117 Valladas, H., Pons-Branchu, E., Dumoulin, J.P., Quiles, A., Sanchidrián, J.L., Medina-Alcaide, M.Á.,
1118 2017. U/Th and 14 C Crossdating of Parietal Calcite Deposits: Application to Nerja Cave (Andalusia,
1119 Spain) and Future Perspectives. Radiocarbon 59, 1955–1967. https://doi.org/10.1017/RDC.2017.120
1120
1121 Van Beynen, P., Bourbonniere, R., Ford, D., Schwarcz, H., 2001. Causes of colour and fluorescence in
1122 speleothems. Chemical Geology 175 (3-4), 319-341. https://doi.org/10.1016/S0009-2541(00)00343-0
1123
1124 Vignaud, C., Salomon, H., Chalmin, E., Geneste, J.-M., Menu, M. 2006. Le groupe des « bisons
1125 adossés » de Lascaux. Étude de la technique de l'artiste par analyse des pigments. *L'Anthropologie*
1126 110 (4): 482–99. https://doi.org/10.1016/j.anthro.2006.07.008.
1127
1128 Watchman, A., 1990. What are silica skins and how are they important in rock art conservation?
1129 Australian Aboriginal Studies 1, 21–29.
1130 *https://search.informit.org/doi/10.3316/ielapa.154935712026809*
1131
1132 Watchman, A., 2000. A review of the history of dating rock varnishes. Earth-Science Reviews 49,
1133 261–277. https://doi.org/10.1016/S0012-8252(99)00059-8
1134
1135 Zhang, X., Tauler, R., 2013. Application of multivariate curve resolution alternating least squares
1136 (MCR-ALS) to remote sensing hyperspectral imaging. Analytica chimica acta 762, 25–38.
1137 https://doi.org/10.1016/j.aca.2012.11.043
1138
1139 Zielinski, R.A., 1980. Uranium in secondary silica; a possible exploration guide. Economic Geology

75, 592–602. https://doi.org/10.2113/gsecongeo.75.4.592

Zielinski, R.A., 1982. Uraniferous opal, Virgin Valley, Nevada: Conditions of formation and implications for uranium exploration. Journal of Geochemical Exploration 16, 197–216. https://doi.org/10.1016/0375-6742(82)90010-3